THESIS FOR THE DEGREE OF LICENTIATE OF ENGINEERING

Novel catalysts development for NO_x reduction from H_2 combustion engines

Jieling Shao

Chemical Engineering Division
Department of Chemistry and Chemical Engineering

CHALMERS UNIVERSITY OF TECHNOLOGY

Gothenburg, Sweden 2024

Novel catalysts development for NO_x reduction from H_2 combustion engines
Jieling Shao

Licentiatuppsatser vid Institutionen för kemi och kemiteknik
Chalmers tekniska högskola.
Nr 2024:01

Department of Chemistry and Chemical Engineering
Chalmers University of Technology
SE-412 96 Gothenburg
Sweden
Telephone + 46 (0)31-772 1000

Printed by Chalmers digitaltryck
Gothenburg, Sweden 2024

Novel catalysts development for NO_x reduction from H_2 combustion engines

Jieling Shao

Department of Chemistry and Chemical Engineering
Chalmers University of Technology, Gothenburg

Abstract

Hydrogen, as a clean energy carrier, burns without producing any carbon emissions. Hydrogen internal combustion engines (H_2-ICE) are considered an alternative for the transition from conventional fossil-fuel vehicles. However, the development of effective aftertreatment catalysts remains necessary to address the inevitable NO_x emissions from internal combustion engines. This thesis covers the performance of various active metals supported on zeolites as catalysts for the selective reduction of NO by H_2 (H_2-SCR), as well as the investigation of the influence of various reaction conditions and the related reaction mechanisms. The results of the thesis work are reported in two manuscripts, namely Paper I and II.

Paper I focus on catalysts with Pt supported on SSZ-13 zeolite. Their performance is evaluated with varying H_2/NO feed ratios (5/10/15), Pt loadings (0.5/1.0/2.0 wt.%), and with and without water co-feeding. Activity tests showed that Pt catalysts have high catalytic activities for H_2-SCR at low temperatures (<150 °C), but only NO oxidation occurs at high temperatures. The reaction process is complex and includes multiple reactions such as competing H_2 oxidation and NO oxidation, as well as other side reactions. The selectivity for the by-product N_2O cannot be ignored and it is even greater than that for N_2 at temperatures less than 120 °C. Higher H_2 concentration promotes N_2 selectivity, and the more exothermic H_2 oxidation aids NO oxidation to occur at lower temperatures. The 0.5 wt.% Pt catalyst was found to possess the highest N_2 selectivity in the loading studies, not only because fewer active sites attenuate the competing hydrogen oxidation reaction, but also it possesses a smaller particle size and higher dispersion, and a larger portion of Pt in its metallic state. Water had a strong inhibitory effect on H_2-SCR at low temperatures, with a significant reduction in N_2 generation compared to anhydrous environments. It was found in in-situ DRIFTS experiments that nitrosyl species weakly adsorbed on the catalyst and could be easily removed; H_2 is absorbed on the Pt active sites and is activated to interact with nitrates. Meanwhile, NH_4^+ ions were formed during the reaction and could play a role as reaction intermediates to assist in the reduction of NO. Simultaneous entry of NO and H_2 induces a faster reaction than sequential entry and affects the binding of surface species, especially NO. The introduction of O_2 to the NO+H_2 mixture generates more nitrite (NO_2^-) species on the catalyst.

Paper II focuses on extending the range of reaction temperatures for H_2-SCR. It was found that Pt/SSZ-13, Pd/SSZ-13, and Ir/SSZ-13 catalyze the H_2-SCR at three temperature intervals, low, medium, and high temperatures, respectively. Also, nitrogen selectivity increases sequentially with temperature. Combining them in series in the order of iridium-palladium-platinum is an interesting option. Due to the low reactivity of Ir, two strategies, a reduction pretreatment and replacement of the support with BETA zeolite, were examined and found to be successful in increasing its nitrogen generation. Similarly, the difference in H_2-SCR reaction properties on the three active centres was investigated using in-situ DRIFTS measurements, and it was found that the Ir had the strongest NO adsorption, which was one of the reasons for its weak activity. No H_2-SCR reaction occurred based on observation from the spectra at 200 °C. After the reduction pretreatment, NO adsorption was weakened due to the metal present more in its metallic state and this contributed to the occurrence of H_2-SCR.

Keywords: H_2-SCR, Platinum, Palladium, Iridium, SSZ-13 zeolite, BETA zeolite, Nitrogen selectivity, in-situ DRIFTS, reduction pretreatment, temperature intervals

Acknowledgements

The work presented in this thesis was carried out at the Division of Chemical Engineering, Competence Centre for Catalysis (KCK), Chalmers University of Technology. The funding by the Swedish Energy Agency and the collaboration with Volvo AB, Scania CV, and Johnson Matthey via a strategic vehicle research and innovation (FFI) project (P51458-1) is greatly acknowledged.

Sincere thanks to Prof. Louise Olsson, Prof. Derek Creaser, and Dr. Phuoc Hoang Ho for their guidance and patience with all my work, especially for my thesis and papers, which also took great effort. And thanks to them for always believing in me and respecting my views on research.

Assoc. Prof. Christine Geers deserves thanks for agreeing to review my thesis, providing invaluable feedback, and engaging in enlightening discussions.

Analysis of the catalysts was mainly carried out at the Chalmers Material Analysis Laboratory (CMAL) and I extend my gratitude for the resources and support provided. Thanks for the assistance with the material characterizations of Dr. Stefan Gustafsson (TEM measurements), Dr. Eric Tam (XPS analysis), and Dr. Andreas Schaefer (CO chemisorption). I am also thankful to Lennart Norberg and Lasse Urholm for their support with the SGB flow reactor.

I would like to thank all my colleagues in the department for their help, for their kindness, and friendliness, and for creating an extremely good working environment for me over the past 2.5 years. Johanna Spång, Anna Oskarsson, and Malin Larsson for all effective administrative support. Michael Andersson-Sarning for the help on chemical purchasing and technical support. Thanks to Wei Di for guiding me to synthesize the zeolite. Special thanks to Sreetama Ghosh, You Wayne Cheah, Phuoc Hoang Ho, Dawei Yao, Rawipa Intakul, Huy Xuan Le, Quoc Khanh Tran, and Emma Olsson Månsson for supporting me not only as a colleague but also as a friend in my life. Thanks also to Mengqiao Di, Alexander Nellessen, and Guido J.L. de Reijer from the Division of Applied Chemistry.

Prof. Gunnar Eriksson, Prof. Claes Niklasson, and Prof. Diana Bernin are acknowledged for their guidance and support in teaching, and my teaching colleagues Aqsa Noreen, Emma Olsson Månsson, Wei Di, Elham Nejadmoghadam, and Alexander Riddell for their cooperation.

Finally, I want to thank my parents and friends for their support and trust in my life and also thank my boyfriend Naichen Wang for his tolerance and companionship.

List of publications

This thesis is based on the following two appended papers.

I. Pt-based catalysts for NO_x reduction from H_2 combustion engines

Jieling Shao, Phuoc Hoang Ho, Wei Di, Derek Creaser, Louise Olsson

Submitted manuscript.

Contribution: Responsible for the design and operation of all experiments, characterization tests (except TEM and ICP), and paper writing.

II. The development of novel catalysts covers the full temperature range of NO selective catalytic reduction by H_2

Jieling Shao, Phuoc Hoang Ho, Derek Creaser, Louise Olsson

Submitted manuscript.

Contribution: Responsible for the design and operation of all experiments, characterization tests (except TEM and ICP), and paper writing.

Publications not included in this thesis:

I have contributed to the X-ray photoelectron spectroscopy (XPS) analysis for the following papers.

I. The effect of Pt/Pd ratio on the oxidation activity and resistance to sulfur poisoning for Pt-Pd/BEA diesel oxidation catalysts with high siliceous content

Phuoc Hoang Ho, **Jieling Shao**, Dawei Yao, Rojin Feizie Ilmasani, Muhammad Abdus Salam, Derek Creaser, Louise Olsson

Journal of Environmental Chemical Engineering, 2022, 10(4): 108217 (https://doi.org/10.1016/j.jece.2022.108217)

II. Role of ZrO_2 and CeO_2 support on the In_2O_3 catalyst activity for CO_2 hydrogenation

Poonam Sharma, Phuoc Hoang Ho, **Jieling Shao**, Derek Creaser, Louise Olsson

Fuel, 2023, 331: 125878 (https://doi.org/10.1016/j.fuel.2022.125878)

III. Role of the supports during phosphorus poisoning of diesel oxidation catalysts

Phuoc Hoang Ho, **Jieling Shao**, Dawei Yao, Wei Di, Derek Creaser, Louise Olsson

Chemical Engineering Journal, 2023, 468: 143548 (https://doi.org/10.1016/j.cej.2023.143548)

IV. Effect of preparation methods on the physicochemical properties of Indium-based catalysts and their catalytic performance for CO_2 hydrogenation to methanol

Phuoc Hoang Ho, Giovanni Tizzanini, Sreetama Ghosh, Wei Di, **Jieling Shao**, Oleg Pajalic, Lars Josefsson, Patricia Benito, Derek Creaser, Louise Olsson

Submitted manuscript.

List of abbreviations

ASC	Ammonia slip catalyst
BET	Brunauer-Emmett-Teller
CEM	Controlled evaporation and mixing system
CI	Compression ignition
DFT	Density functional theory
DPF	Diesel particulate filter
DOC	Diesel oxidation catalyst
DRIFTS	Diffuse reflectance infrared Fourier transform spectroscopy
FCV	Fuel cell vehicle
FTIR	Fourier-Transform infrared spectroscopy
GHG	Greenhouse gas
HAADF	High-angle annular dark-field
HRTEM	High-resolution transmission electron microscopy
ICE	Internal combustion engine
ICP	Inductively coupled plasma
MFC	Mass flow controller
MS	Mass spectrometry
PI	Positive ignition
SCR	Selective catalytic reduction
SGB	Synthetic gas bench
STP	Standard temperature and pressure
TOF	Turnover frequency
XPS	X-ray photoelectron spectroscopy
XRD	X-ray diffraction

Contents

1 Introduction

1.1 H_2 internal combustion engines (ICE)

The combustion of conventional gasoline and diesel fuels in ICEs, produces not only NO_x but also toxic and harmful gases such as CO and HC, and CO_2, which is a prominent greenhouse gas (GHG). Since 2019, the EU has progressively issued regulations targeting CO_2 emissions for new cars and vans including Regulation (EU) 2019/631 and Regulation (EU) 2023/851 as well as 'the European Green Deal'. It proposed that the EU's greenhouse gas emissions should be reduced by at least 55% by 2030 and zero net emission of GHGs reached by 2050. Therefore, technologies using renewable and non-carbon-based energies have been subject to large development. Hydrogen as a carbon free energy source, is an advantageous fuel as it can provide efficient and eco-friendly energy production. Compared to nearly all other fuels, hydrogen has a wide flammability range in air (4-74% vs. 1.4-7.6% for gasoline) which implies a wide range of fuel-air mixtures are possible for combustion.[1] Hydrogen also has a very low ignition energy that enables a greater fuel economy due to a more complete combustion of the fuel [2,3]. However, topics such as the hydrogen storage and transport, engine-design and hydrogen refueling stations all remain challenging and under development [4]. Still, H_2-ICE vehicles can be very important for the future [5]. In principle, nitrogen oxides (NO_x) are the only undesirable engine out emissions from hydrogen combustion engines [6]. It is therefore crucial to efficiently remove the NO_x.

1.2 Nitrogen oxide emissions

Nitrogen oxides including NO, NO_2, N_2O and their derivatives have negative impact on health, the environment, and biological ecosystems. NO is very easily oxidised to NO_2, and the strong acidity from NO_2 results in acidification and eutrophication of land and water[7]. N_2O, the third most important greenhouse gas, also substantially contributes to global warming. Nitrogen oxides are formed when nitrogen and oxygen react at high temperatures. Man-made emissions of nitrogen oxides dominate total emissions in Europe. The sources include automobiles, trucks and various non-road vehicles as well as stationary industrial sources [8]. According to a report from United States Environmental Protection Agency[9], NO_x emissions generated from on-road diesel/gasoline combustion in New England, USA, account for a total of 47% of NO_x emissions, see **Fig. 1** below. Although each country's situation is different, the European Environment Agency reported that in 2011[10], the most significant sources of NOx emission were 'Road transport (41%)', and similarly, the transport sector is the single largest source of nitrogen oxides in Sweden[11].

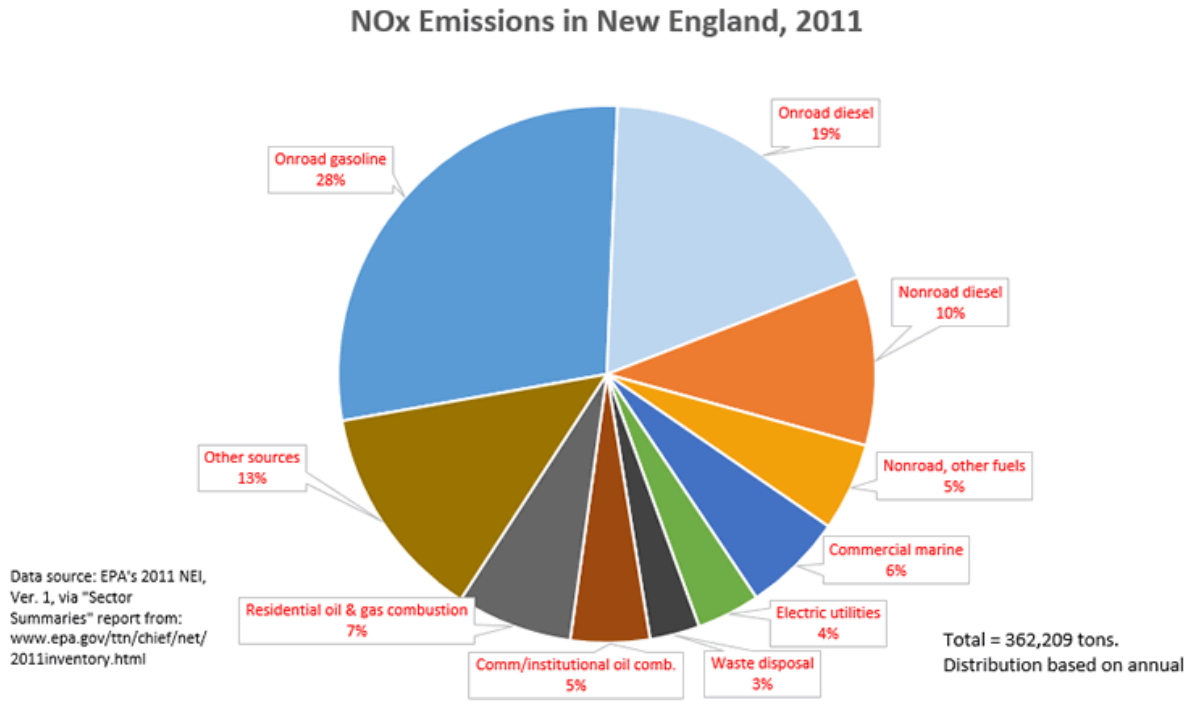

Fig. 1. The pie chart of NO_x emissions in New England distributed among various sectors in 2002. (https://www3.epa.gov/region1/airquality/nox.html)

1.3 NO_x emission standards

As mentioned before, most of the world's NO_x emissions come from transport, so this section focuses on the control of tailpipe emissions. Tailpipe emission standards were first introduced in California in 1959 to control CO and HC emissions from gasoline engines. Currently, California's emission standard remains among the most stringent, while EU has issued six versions of emission regulations (Euro I – Euro VI) for both gasoline passenger cars and light duty vehicles and diesel heavy-duty trucks & bus vehicles. NO_x is one of the strongly regulated exhaust components in addition to carbon monoxide (CO), hydrocarbon (HC), particulate matter (PM) and particle number (PN). Also, emission limits for NO_x have become progressively stringent with each version of regulations (**Table 1**). As a result, higher demands are being placed on NO_x emission control to cope with stricter emission regulations. **Figure 2** shows NO_x emissions in Sweden from 1990 to 2021, with a decreasing trend from year to year. Since 1990, the legislation for emissions of nitrogen oxides from domestic traffic has fallen by 72%, while total NO_x emissions have been reduced by more than half (**Table 1**).

Table. EU emission standards for heavy-duty CI (diesel) and PI engines: Transient testing (https://dieselnet.com/standards/eu/hd.php) CI- compression ignition; PI- positive ignition.

Stage	Date	Test	CO	NMHC	CH_4[a]	NOx	PM[b]	PN
			g/kWh					*1/kWh*
Euro III	*1999.10 EEV only*	ETC	*3.0*	*0.40*	*0.65*	*2.0*	*0.02*	
	2000.10		5.45	0.78	1.6	5.0	0.16[c]	
Euro IV	2005.10		4.0	0.55	1.1	3.5	0.03	
Euro V	2008.10		4.0	0.55	1.1	2.0	0.03	
Euro VI	2013.01	WHTC	4.0	0.16[d]	0.5	0.46	0.01	6.0×10^{11}[e]

[a] for gas engines only (Euro III-V: NG only; Euro VI: NG + LPG)
[b] not applicable for gas fueled engines at the Euro III-IV stages
[c] PM = 0.21 g/kWh for engines < 0.75 dm^3 swept volume per cylinder and a rated power speed > 3000 min^{-1}
[d] THC for diesel (CI) engines
[e] PN limit for PI engines applies for Euro VI-B and later [EC 2014]

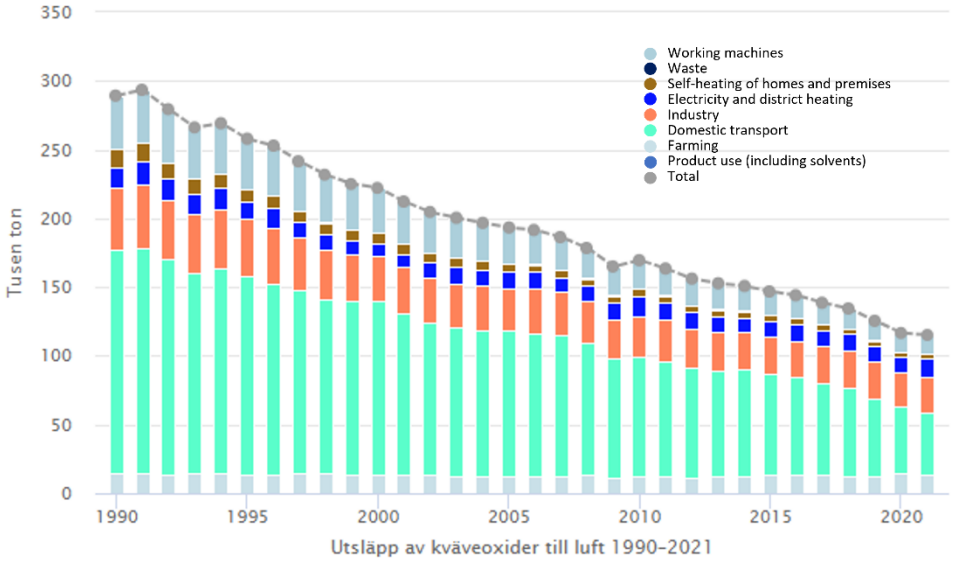

Fig. 2. NO_x emissions to air in the period of 1990-2021 in Sweden. (https://www.naturvardsverket.se/data-och-statistik/luft/utslapp/utslapp-av-kvaveoxider-till-luft/)

1.4 NO_x emission control

Regardless of the fuel, during high temperature combustion with air in an internal combustion engine, NO_x generation is unavoidable. Many efforts have been made to control the NO_x emissions by post-combustion removal processes. Selective catalytic reduction (SCR) technology is one of the advanced, economical technologies for the abatement of NO_x from diesel engine emissions. For conventional diesel internal combustion engines (ICE), ammonia (NH_3)-assisted SCR systems are used to achieve a de-NO_x function. They are positioned (for a typical EuroV heavy-duty engine) after a diesel oxidation catalyst (DOC), and diesel particulate filter (DPF), but before an ammonia slip catalyst (ASC)[12]. NH_3-SCR was patented in the United States by the Engelhard Corporation in 1957 [13,14]. It has been introduced in the automotive industry in later years to cope with the stringent regulations on NO_x emissions [15]. Ammonia as a reducing agent is produced by the decomposition of injected urea and mixed with other gases into the SCR catalyst. However, the design of the injection equipment is complex to ensure proper atomization to calibrate a stoichiometric NH_3/NO injection and to prevent urea crystallization. Some drawbacks, such as ammonia slip, high operating cost, and crystallization byproducts cause equipment fouling and corrosion problems [16]. For hydrogen fueled engines, H_2-SCR is an interesting NO_x abatement strategy, since it does not require an additional ammonia reservoir and injection system. Recently, hydrogen used as the reducing agent has attracted more and more attention for NO_x removal because it provides a promising way to meet the emission limits without inducing secondary pollutants [17–19]. However, H_2-SCR catalysts examined in the literature have lower activity and selectivity compared to conventional NH_3-SCR.

Here, the definition of catalyst needs to be re-emphasised. A catalyst is a substance that increases the rate of a chemical reaction by lowering the activation energy required for the reaction to occur, without itself being consumed or permanently altered in the process. To accelerate the reaction, it does participate in the reaction process by forming bonds with the reactants, allowing them to react to a product, which detaches from the catalyst and leaves it unaltered. With the participation of the catalyst, the reaction undergoes an alternative path but energetically more favorable, namely the catalyst lowers the activation energy barrier it needs to overcome. However, the change in the Gibbs free energy between the reactants and products does not change with a catalyst, so the catalyst does not affect the equilibrium of the reaction. Theoretically, if a reaction is thermodynamically unfavorable, then a catalyst cannot make the reaction happen; a catalyst only changes the kinetics and not the thermodynamics[20]. The catalysts used for H_2-SCR are typical heterogeneous catalysts, with the solids catalysing the gas phase reactions. The catalyst consists of an active site and a porous high surface area carrier. Although catalysts have an accelerating effect on reactions, different active sites catalyse to different degrees, i.e. catalytic activity. And the reaction process is complex, generating a variety of by-products, so the selectivity of the reaction target product N_2 is also extremely important.

1.5 Objectives and scopes of the thesis

The purpose of this work is to develop a high-efficient catalyst for selective reduction of NO by H_2 with both high activity - NO conversion and high selectivity for N_2. Several active metals have been synthesized and screened for H_2-SCR, where their activity performance and reaction condition optimization were evaluated. To fully understand the reaction pathway, a preliminary mechanism has been studied on different catalysts.

In **Paper I**, Pt-based catalysts with three loadings (0.5/1.0/2.0 wt.%) supported on a lab-synthesized SSZ-13 zeolite were prepared. Activity evaluations of the Pt/SSZ-13 samples under different conditions including H_2/NO ratio, Pt loadings and w/o H_2O were compared, and multiple characterization measurements of the catalysts were carried out to interpret the results. The reaction processes within specific temperature regions were described according to the activity test results and insights into the reaction mechanism were revealed by carefully designing DRIFTS measurement to exclude the effect of water.

Paper II is a communication paper. It describes the activities of H_2-SCR on Pt/Pd/Ir catalysts supported on SSZ-13 zeolite and their combinations. It was found that the three active metals have their specific working temperature windows that can cover a wide temperature range of H_2-SCR. Two strategies that included reduction pretreatment and changing to a BETA zeolite support for the Ir catalyst could successfully improve its reactivity. XPS characterization and DRIFTS measurements revealed reasons for the different performances for H_2-SCR of the three metals.

1.6 Outline of the thesis

The outline of this thesis is as follows:

Chapter 1: General introduction of the background, motivation, and objectives.

Chapter 2: Introduction of H_2-SCR mechanism, H_2-SCR catalysts and their challenges.

Chapter 3: Description of catalyst synthesis, activity tests and characterization methodology.

Chapter 4: Key findings of **Paper I** and **Paper II** and interpretations.

Chapter 5: Main conclusions.

Chapter 6: Future work.

2 Background

2.1 H_2-SCR catalysts

2.1.1 Reaction mechanism

The reaction process of NO and H_2 under excess O_2 conditions is very complex, if only considering the reaction between two gases, the following reactions can occur:

$2H_2 + 2NO \rightarrow N_2 + 2H_2O$ (1)
$H_2 + 2NO \rightarrow N_2O + H_2O$ (2)
$O_2 + 2H_2 \rightarrow 2H_2O$ (3)
$2NO + O_2 \leftrightarrow 2NO_2$ (4)
$2NO + 5H_2 \rightarrow 2NH_3 + 2H_2O$ (5)

Reaction (2) indicates that N_2O is a by-product formed by NO reacting with H_2. H_2 oxidation (3) is a competing reaction during H_2-SCR under conditions with O_2 which not only leads to a lower utilization of the reactant H_2, but also affects the temperature profile by the exothermic reaction. If H_2 oxidation is combined into reactions (1) and (2), as suggested by Costa et al. using a Pt-supported catalyst [21]:

$2NO + 4H_2 + O_2 \rightarrow N_2 + 4H_2O$ (ΔH= -573.7 kJ/mol NO) (6)
$2NO + 3H_2 + O_2 \rightarrow N_2O + 3H_2O$ (ΔH= -411.9 kJ/mol NO) (7)
$1/2O_2 + H_2 \rightarrow H_2O$ (ΔH= -271.7 kJ/mol H_2) (8)

It was demonstrated that the reaction (6) was the energetically most favorable reaction among the three reactions ($\Delta G = \Delta H - T\Delta S$; G – Gibbs free energy; H – enthalpy; S - entropy). According to reactions (4) and (5), by-products such as NO_2 and NH_3 can be formed as well. Here, NO_2 formation may have an inhibition effect on NO reduction by H_2, since NO_2 itself has a strong oxidizing activity. Opposite to this, ammonia produced by reaction (5) could play a positive role in aiding the NO reduction following the NH_3-SCR mechanism.

The detailed reaction mechanism can be divided into NO adsorption/dissociation and oxidation/reduction parts. In terms of the NO adsorption/dissociation, NO firstly adsorbs on the active metal (Pt, Pd, etc.) or the support surface. Among the multiple elementary steps, NO dissociation to N_{ad} and O_{ad} is considered to be the key step to produce adsorbed N atoms, and the subsequent formation of N_2. Hydrogen is also absorbed on the catalyst surface and dissociated to form active H_{ad} atoms. The role of the H_{ad} atoms is to remove the O_{ad} from the active sites and assist the NO dissociation [22,23]. This is confirmed by the work from Bell and Hecker that the energy needed for forming N_{ad} from N-O bond dissociation is higher than that from N-O-H dissociation [24,25]. Papp and Sabde found that when the hydrogen was cut off, N_2O was generated while the N_2 formation dropped, and they proposed that the mechanism for N_2O formation involves neighboring NO_{ad} and O_{ad} since O_{ad} could be removed in the absence of H_2 [26]. This demonstrates the negative effect of O_2 because the oxygen-covered active site inhibits the NO adsorption and excess oxygen consumes the reducing agent hydrogen [27].

The oxidation-reduction mechanism is more complicated regarding the active reaction intermediates. Shibata et al have proposed a mechanistic scheme for H_2-SCR on Pt catalysts as

shown in **Scheme 1** [28]. H_2 firstly adsorbs on the metallic Pt surface and dissociates to form active H_{ad} atoms that assist the NO dissociation to generate N_{ad} and O_{ad}. O_{ad} can react with H_{ad} to produce water. N_{ad} can react with another N_{ad} to form N_2, with NO to form N_2O and with H_{ad} to form NH_x which is one active intermediate to further react with H_{ad} to form NH_3. Another pathway for the N_2 formation involves NO_{ad} reacting with H_{ad}. The NH_x as an intermediate existing on Pt(100) is also reported by some other researchers [29]. These species could play a role as reducing agents that further reduce the NO to produce N_2 and N_2O. NH_3 can be stored on the Brønsted sites of the support as NH_4^+ which can have the same function as NH_x(ad).

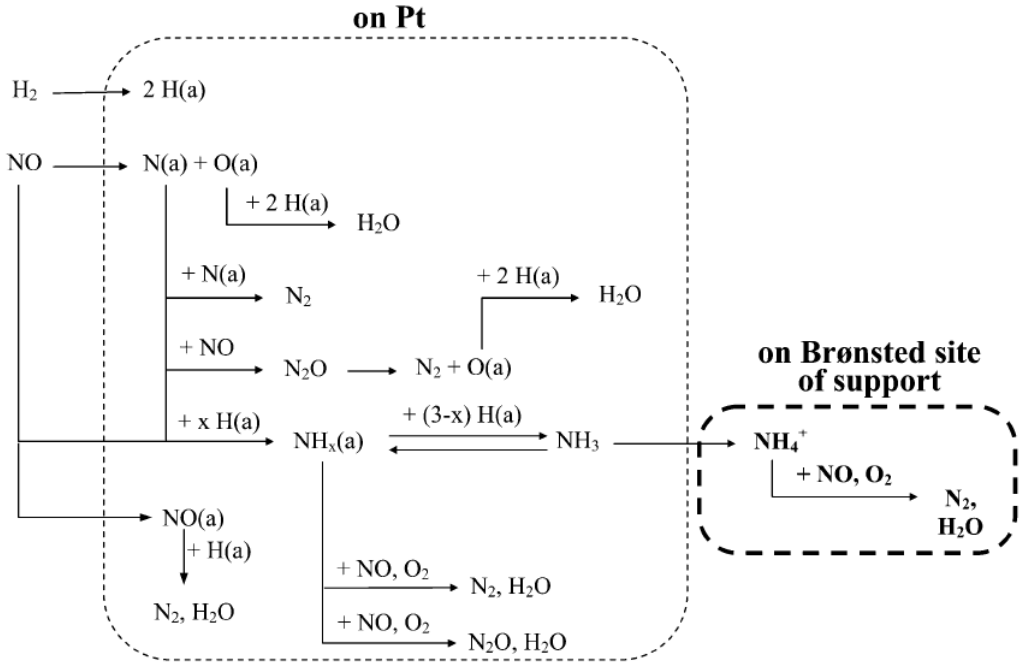

Scheme 1. Proposed mechanism for SCR by H_2 over Pt catalysts. Reprinted with the permission from ref. [28]. Copyright (2004) American Chemical Society.

Regarding the N_2O formation mechanism, Zhang and co-workers have investigated it with a Pt/HY catalyst [30]. The overall reaction process in **Fig. 3** is similar to that in **Scheme 1**. The mechanism for the N_2O formation has the following two routes:

On Pt surface: $H_{(ad)}$ + nitrous species$_{(ad)}$ + $O_{2(ad)}$ → N_2 + N_2O + H_2O (9)

At Pt-support interface: $H_{(spillover)}$ + nitrous species$_{(ad)}$ → N_2O + N_2 + H_2O (10)

Since N_2 was formed by an adsorbed H atom ($NO_{ad}+H_{ad}\rightarrow N_{ad}+OH_{ad}$), the relative quantity of H_{ad} with respect to nitrous species on the Pt surface is a key point in reaction (9). It was also claimed that H is involved in spillover as in reaction (10) which was supported by the work of Conner et al. and Shin et al. [31,32]. Nevertheless, H spillover requires overcoming certain energy barriers, often resulting in insufficiently active H at the Pt and support interface. It tends to form the by-product N_2O by $N_{(ad)}+NO_{(ad)}\rightarrow N_2O$.

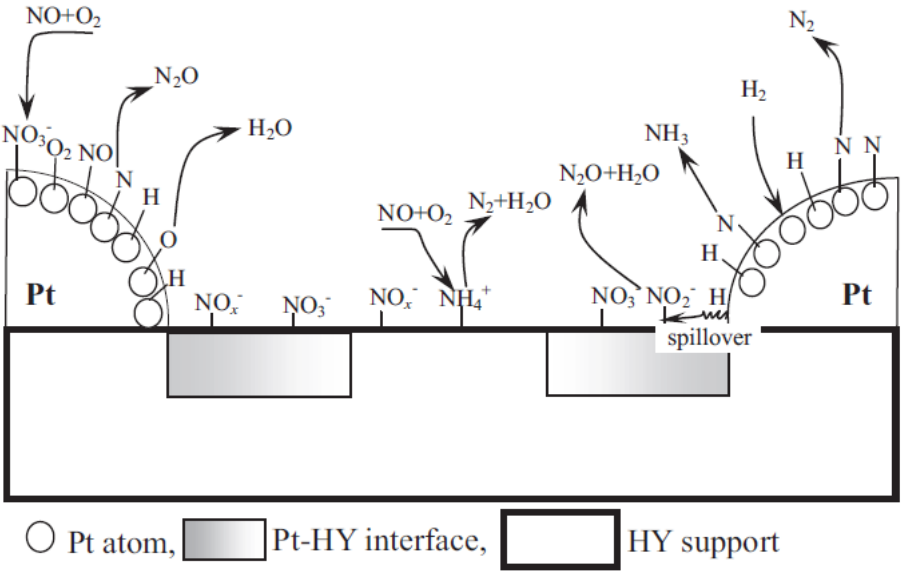

Fig. 3. N_2 and N_2O formation routes on Pt surface and at Pt-HY interface. Reprinted with the permission from ref. [30]. Copyright (2014) Elsevier.

It was also reported in several publications that the reaction pathway is also dependent on the reaction temperature [33,34]. Komatsubara et al. have proposed the following reaction pathways, based on different temperature regions with a Pt/Nb-AlMCM-41 catalyst [35]:

At 313-373 K

$2NO \rightarrow N_2O + O_{ad}$ (11)

$O_{ads} + H_2 \rightarrow H_2O$ (12)

At 350-450 K

$2NO + 5H_2 \rightarrow 2NH_3 + 2H_2O$ (13)

$4NO + 4NH_3 + O_2 \rightarrow 4N_2 + 6H_2O$ (14)

$4NO + 4NH_3 + 3O_2 \rightarrow 4N_2O + 6H_2O$ (15)

At 450-650 K

$2NO + 5H_2 \rightarrow 2NH_3 + 2H_2O$ (16)

$4NH_3 + 3O_2 \rightarrow 2N_2 + 6H_2O$ (17)

$2NH_3 + 2O_2 \rightarrow N_2O + 3H_2O$ (18)

According to this mechanism, at low temperature, H_2 removes oxygen from the Pt surface to regenerate the active site. N_2O was the dominant product at low temperatures (<373 K). With increasing temperature, NH_3 forms and becomes an important intermediate[36], reacting with NO and O_2 to generate the N_2 and N_2O. Similarly at the highest temperature range of 450-650 K, NO was reduced to form NH_3 that subsequently tended to undergo oxidation reactions.

Summarising the above reaction mechanisms, including NO adsorption/desorption as well as metal redox states, it is evident that hydrogen probably not only plays the role of a reducing agent, but also removes oxygen from the metal surface and assists in the dissociation of NO, and the possibility of hydrogen spillover onto the support should not be ignored. Oxygen, on

the other hand, plays a negative role, not only consuming hydrogen excessively, but also competing for adsorption on the active metal surface to inhibit the reaction. In addition, NH_x is an important reaction intermediate that can assist in the reduction of NO. However, it should be noted that the exact mechanistic steps of the reaction are complex and can vary depending on the specific catalyst material and reaction conditions.

2.1.2 Pt-based catalysts

Following the above discussion, most of the reaction mechanisms were investigated on the surface of platinum-based catalysts due to the fact that platinum group metals, in particular Pt and Pd, have been found to be the most active compared to other catalysts for NO_x reduction by H_2 [19,37]. During 20 years of research, many scholars have found that platinum has a high NO conversion for this reaction in the low-temperature range of 100-200 ℃, but also with N_2O formation as the main by-product [38,39]. Jones et al. first reported the possibility of use of Pt as a H_2-SCR catalyst in 1971 [40]. Fu and Chuang have confirmed that Pt has the best activity among precious metals for H_2-SCR in the order Pt>Pd-Ru>Pd>Ru>>Au [41]. It has been reported in one publication that NO starts to be reduced from 40 ℃ and reaches a maximum NO conversion of 75% at 90 ℃ on a Pt/SiO_2 catalyst [42].

Costas and co-workers have studied Pt supported on various metal oxides (Al_2O_3, SiO_2, La_2O_3, MgO, Y_2O_3, CaO, CeO_2, TiO_2 and MgO-CeO_2), and found that among different catalysts, Pt/MgO and Pt/CeO_2 showed good catalytic activity and the binary oxide of 50 wt.% MgO- 50 wt.% CeO_2 was the best [21,43]. Yokota et al. investigated NO_x removal with H_2 in the presence of an excess of oxygen on Pt catalysts. The results showed the effectiveness of the catalyst support was in the order of ZSM-5~mordenite>SiO_2>Al_2O_3 [44]. It was shown that activity for NO conversion and N_2/N_2O selectivity were strongly dependent on the support for the Pt catalysts. Some works have reported that Pt supported on HY [45], HZSM-5 [46,47], HMCM-41 [48], and HFER[49] zeolites were highly active for H_2-SCR due to the large surface area and the appropriate acidity, which is beneficial for the N_2 selectivity [50]. Additionally, Shibata et al. found that the N_2 selectivities for Pt/zeolites were generally higher than those on Pt/metal oxides and were in order of Pt/MFI > Pt/BEA > Pt/Y, Pt/MOR [28]. Yokota et al. also reported that Pt-ZSM was more active than Pt/SiO_2 and Pt/γ-Al_2O_3 [51]. In another work, Li et al. found that Pt-Ti-MCM-41 exhibited good stability and tolerance against SO_2 and CO [48]. In fact, most of these reports on zeolites having better reaction selectivity take into account their acidic nature, in addition to the influence of the interaction of the active metal and the support, the dispersion of the active metals on the support and the morphological structure of the zeolite themselves. Briefly, the reaction mechanism mentioned in the previous section indicates the formation of the important intermediates NH_x during the reaction, which can be adsorbed on the acid centres of the carrier to assist in the reduction of NO [52].

In addition, there is a lot of work directed towards the effect of promoters on platinum catalysts. Sodium (Na) as a promoter, added in minute quantities to Pt/ZSM-15 and Pt/Al_2O_3 catalysts, has been found to increase Pt^0 generation, favoring the H_2-SCR activity and selectivity. It has to be mentioned here that the redox properties of active metals are crucial for the reaction and not only for the Pt. It has been demonstrated in the literature [53] that the predominant mechanism is decomposition of NO on reduced Pt metal sites, followed by the regeneration of the active Pt

sites by the reductant. Oxygen adsorbed on the Pt surface has inhibition effect of the NO adsorption and further reaction, as well as the H_2 dissociation[54]. In another paper, the addition of tungsten oxide (WO_3) has demonstrated remarkable enhancement in activity within the low temperature range of 100-175 ℃, when 0.5% was added to Pt/TiO_2 [55]. The addition of 1% WO_3 resulted in the increase of NO conversion from 35% to 86% at 150 ℃. Further increasing the loading of WO_3 to 2%, the activity window shifted to lower temperature and the NO conversion was enhanced and resulted in 88% at 125 ℃. The enhancement of low-temperature activity was suggested to be due to electron transfer from WO_3 to Pt sites, which led to the formation of metallic Pt.

2.1.3 Pd-based catalysts

Opposite to the catalyst performance of Pt-based catalysts, Pd-based catalysts are attractive for NO reduction with higher N_2 selectivity. It was reported that Pd catalysts supported on oxides showed much better nitrogen selectivity than Pt-based catalysts, which could obtain over 95% NO conversion and above 80% N_2 selectivity at 200 ℃ [56]. Ueda et al. reported that there is a second NO conversion peak on Pd-oxides (supported on Al_2O_3, TiO_2) at 300 ℃ compared to Pt-oxides which indicated that Pd has activity at higher temperature [18]. In 2002, Wen found that Pd/MFI had a high N_2 selectivity of 70% at 100 ℃. N_2 was the only N-containing product without any N_2O formation. The oxidation of Pd^0 and the agglomeration of PdO are responsible for decreased NO reduction activity at high temperatures (>200 ℃)[57].

It should be noted that the exhaust of a hydrogen internal combustion engine contains a higher concentration of water than conventional fuels (e.g. at air/fuel = 1, the molar fraction of water is 34% in the exhaust)[58,59], so the study of the subsequent effect of water on H_2-SCR catalysts is important. Engelmann-Pirez and coworkers have investigated the water effect on Pt and Pd supported on Al_2O_3 and $LaCoO_3$. The most prominent result obtained was that for $Pd/LaCoO_3$, different from other catalysts, water had a promotional effect on NO reduction without affecting the selectivity behavior. Whereas water had a strong inhibiting effect on the rate of H_2-SCR for Pd/Al_2O_3 and Pt catalysts. It was explained by a probable stabilizing effect of water on the metallic character of Pd, due to interactions between Pd and $LaCoO_3$ perovskite [56]. This discovery indicates at the same time, that the support probably has an important influence on the reaction performance. Qing et al. have studied Pd on Al_2O_3, SiO_2 and MgO, and they found that Pd/Al_2O_3 and Pd/SiO_2 exhibited high activities, gaining 100% NO_x conversion above 200 ℃, however, there is no activity on Pd/MgO [60]. Moreover, studies related to promoter effects have also been done on many Pd-based catalysts. According to the work from Leicht et al., a novel $Pd/WO_x/ZrO_2$ catalyst with a W promoter content of 8.7% showed considerable H_2-deNO_x activity between 125 and 280 ℃, with an outstanding overall N_2 selectivity of 96%, due to the increased electron density on Pt caused by the tungsten promoter. Mechanistic studies conducted by DRIFTS spectroscopy indicated that the reaction occurs on the Pd sites, and the formed water mainly adsorbed on the WO_x which reduced the inhibition of the Pd surface [61,62]. It has also been reported that Mn as an additive on Pd/TiO_2-Al_2O_3, not only enhanced the activity performance, but also remarkably increased N_2 selectivity above 150 ℃. The synergetic effect between Pd and Mn led to more NO_x adsorbed in new types of nitrite and nitrate species which were considered more reactive in the H_2-SCR process [63].

In addition, Savva et al. investigated the impact of Pd particle size (ca. 13-45 nm) on H_2-SCR performance within the 130-220 °C temperature range. They observed a substantial increase in the rate of NO conversion with smaller Pd particles. This enhancement was attributed to an increased concentration of active NO_x formed in the vicinity of the Pd-ceria interface (**Scheme 2**) and an accelerated rate of H-spillover. According to the literature, the Pd surface is expected to accommodate $H_{\text{-surface}}$ and $O_{\text{-s}}$ under H_2-SCR reaction conditions, and likely inactive $NO_{x\text{-s}}$ [64,65]. The active NO_x was located within a zone around the Pd nanoparticles. The CeO_2 support has influence on the dispersion and stabilization of deposited Pd metal, activation of NO_x, H-spillover rate and the oxidation of Pd particles [66–68]. Consistent with the coverage of the NO_x, TOF_{NO} (s^{-1}) was notably higher over the small Pd particles than on the larger particles [69]. Part of the adsorbed NO_x might be inactive. The surface coverage of the active adsorbed NO_x species was 10 times larger for the smaller particles (13 nm) compared to the large particles (45 nm). This disparity was attributed to a significant portion of the active NO_x species concentrated in the region surrounding the Pd nanoparticles, where the diffusion rate of hydrogen from the Pd surface towards the interface played a crucial role.

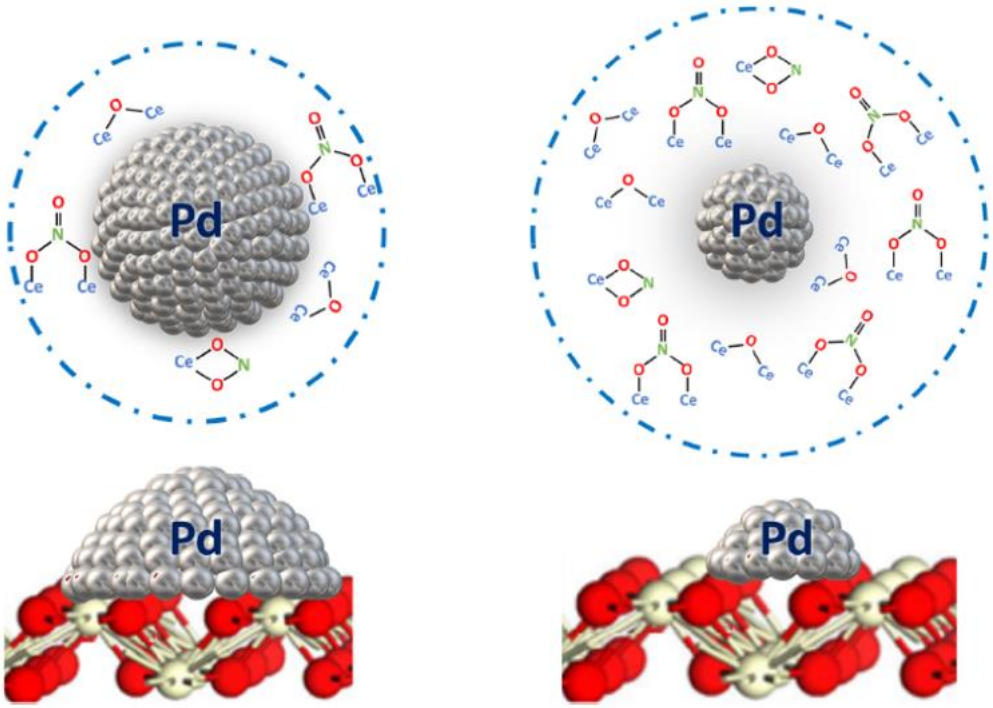

Scheme 2. Dependency of the extent (Δx, nm) of reaction zone of active NO_x-s formed in the H_2-SCR on Pd particle size for the Pd/CeO_2 catalytic system. Reprinted with the permission from ref. [69]. Copyright (2021) Elsevier.

2.1.4 Ir-based catalysts

Apart from Pt and Pd, Ir has been reported to have two advantages, namely higher N_2-selectivity and high-temperature catalytic properties. In particular, Ir-based catalysts can still convert NO to N_2 at high temperatures (>300 ℃) under an oxygen environment when the catalyst surface is dominated by oxygen [70]. There seems to be a certain academic consensus on the performance of Pt and Pd on H_2-SCR, but interestingly there are still discrepancies for Ir due to the more limited studies of Ir-based catalysts. Burch et al. reported that Ir had no activity for H_2-SCR [42]. By contrast, Nanba and co-workers demonstrated that Iridium exhibited definite activity, although lower than Pt or Pd [52]. Yoshinari et al. reported excellent NO conversion to N_2 on Ir/SiO_2 catalyst in the absence of O_2 at higher temperatures (>300 ℃) [71]. However, in the presence of oxygen, the NO reduction was decreased. Surprisingly, the presence of SO_2 has a considerable effect on changing the situation of Ir/SiO_2 under the strong inhibition by excess oxygen. The promoting effect of SO_2 over Ir/SiO_2 is not only found for H_2-SCR but was also observed for CO-SCR and various hydrocarbons from Yoshinari's other studies [72]. Providing some insight into the reasons, SO_2 showed an inhibiting effect on NO reduction in the absence of O_2. The coexistence of O_2 and SO_2 was essential for NO reduction to occur faster (**Fig. 4**). It has been observed by FTIR that in the absence of SO_2, O_2 inhibited the formation of NH_x which is considered an important intermediate to reduce NO. However, in the absence of O_2, NO reduction was completely inhibited due to the strong SO_2 adsorption on the Ir surface. Finally, in the co-existence of O_2 and SO_2, O_2 can be removed by SO_2 oxidation, and more vacant Ir surface sites were created to allow NO adsorption and further reaction.

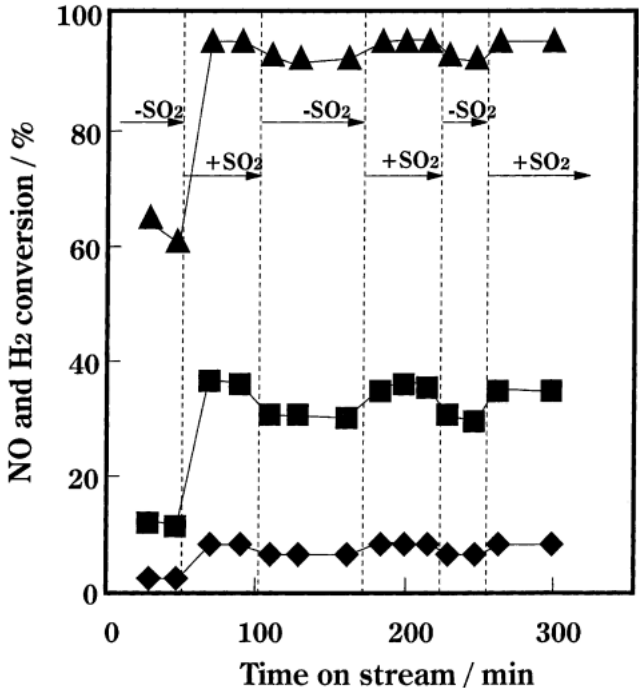

Fig. 4. Response of NO and H_2 conversion to intermittent feed of SO_2 over 0.5% Ir/SiO_2 catalyst. Conditions: NO=1000 ppm, O_2=0.65%, H_2O=10%, H_2=3000 ppm, SO_2=0 or 20 ppm, T =400 ℃, W/F=0.0267 g s cm^{-3}. (■) NO conversion to N_2, (♦) NO conversion to N_2O, (▲) H_2 conversion. Reprinted with the permission from ref. [72]. Copyright (2003) Elsevier.

Regarding the mechanism on the Ir catalyst, four elementary reactions, namely NO dissociation, N_2O formation and NO_2 formation were investigated on the flat (111) and the stepped (211)

surfaces of iridium. It was found by DFT calculations (**Table 1**) that step-Ir sites can generally bond NO, N and O more strongly which was related to the lower coordination of metal atoms at step edges than those at flat surfaces. **Table 1** also displays the barriers of NO dissociation and N_2 formation on step Ir(211) than on the flat Ir (111) surfaces. Since on Ir (211), the barriers for the reactions followed the order: NO dissociation < N_2 formation < N_2O formation < NO_2 formation, high N_2 selectivity could be achieved by controlling the temperature to only produce N_2. All the data reveals that the reaction is dependent on the structural sensitivity of the Ir surface. Since both temperature and water vapour effects during the reaction change surface structure, it has been suggested that smaller particle size Ir catalysts could be used to increase the step facets, thus increasing the nitrogen selectivity [73].

Table 1. Calculated adsorption energies (E_{ad})[a] of NO, N, and O on the most stable sites, and the barriers (E_a) for the elementary reactions on Ir and Pt. Reprinted with the permission from ref. [73]. Copyright (2003) American Chemical Society.

		Ir {211}	Ir {111}	Pt {211}	Pt {111}
E_{ad}	NO	3.14	2.10	2.44	2.05
	N	5.51	5.16	4.50	4.45
	O	5.39	4.73	4.31	4.00
E_a	$NO \rightarrow N + O$	1.19	1.46	1.70	2.60
	$N + N \rightarrow N_2$	1.81	2.60	1.07	2.72
	$NO + N \rightarrow N_2O$	2.31	1.33	1.66	1.78
	$NO + O \rightarrow NO_2$	2.56	1.46	1.95	1.52

[a] The units are eV.

2.1.5 Summary of metal catalysts

The performance of Pt, Pd and Ir catalysts are described above, and it is easy to conclude that the different active metals have their own characteristics; Pt has the highest NO conversion and the reaction occurs at low temperatures (<150 ℃), Pd is in the middle of the temperature range (100-300 ℃) and the NO conversion is relatively lower than that of Pt, and Ir catalysts have lower activity, mainly present at high temperatures (>300 ℃). The predominant formation of the by-product N_2O is inevitable on Pt catalysts at low temperatures, but the selectivity to N_2 is better on Pd and Ir catalysts. Undoubtedly, improvements can be made by support effects, promoter effects, multi-metal synergistic interactions and different reaction conditions. The authors in one literature report concluded that the nature of the noble metals is affected by the working temperature [52].

Upon reviewing the literature on the reaction mechanism, the significance of competitive H_2 oxidation activity at varying temperatures on the catalyst becomes evident. Consequently, this thesis work is committed to two primary goals: identifying an optimal active center and evaluating its impact on enhancing the catalyst. Ultimately, the aim is to create a catalyst that efficiently achieves superior N_2 selectivity across a broader range of temperature intervals.

3 Experimental

This chapter of the thesis describes the methods used for catalyst synthesis, catalyst characterization methods and catalytic activity measurements for both studies.

3.1 Catalyst synthesis

3.1.1 SSZ-13 zeolite synthesis

The Na-SSZ-13 zeolite was prepared by a hydrothermal synthesis method. Firstly, a gel was mixed with the following molar composition: $0.1Na_2O$: $1SiO_2$: $0.025Al_2O_3$: 0.2N,N,N-trimethyl-1-adamantylammonium hydroxide (TMAdOH):$44H_2O$ [74]. The sodium, aluminum and silica sources and the zeolite morphology template were sodium hydroxide (VMR Chemicals), aluminium hydroxide hydrate (Sigma-Aldrich), fumed silica (Sigma-Aldrich), and TMAdOH (TCI), respectively. The mixture has been stirred and aged overnight at room temperature to form a uniform gel. Then it was transferred to a Teflon-lined stainless-steel autoclave and was kept in a rotating oven under the conditions of 160 ℃ for 6 days to form the zeolite structure. After 6 days, when the autoclave cooled down to room temperature, it could be opened. The solution from the autoclave was centrifuge-washed several times with Milli-Q water and then dried at 80 ℃ overnight. The solid sample was ground to powder and calcined to fully remove the template organic compounds at 600 ℃ for 8 h. The Na-SSZ-13 was obtained after calcination.

The H-SSZ-13 was obtained by an ion exchange method from Na-SSZ-13. The Na-SSZ-13 powder was stirred with 0.5 M NH_4NO_3 (Thermo Scientific) solution (100 mL per 1 g powder) at 80 ℃ for 2 h, and then washed with Milli-Q water until pH value around 7 was reached. This procedure was repeated twice to ensure adequate exchange. After that, the sample with ammonium form was dried overnight at 80 ℃ and calcined at 550 ℃ for 6 h to change to the proton type SSZ-13 zeolite.

3.1.2 Pt, Pd, Ir catalyst preparation

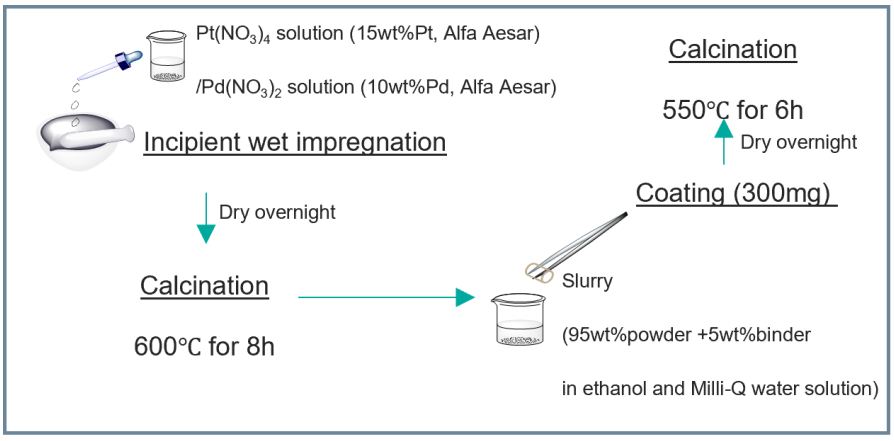

Fig. 5. Synthesis procedure of catalysts and monoliths.

As illustrated in **Fig. 5**, the monometallic Pt/Pd/Ir supported on SSZ-13 zeolite catalysts of 1 wt.% loading was prepared by an incipient wetness impregnation technique. Pt or Pd solution was prepared by mixing $Pt(NO_3)_4$ precursor (Alfa Aesar, 15 wt.% Pt) or $Pd(NO_3)_2$ precursor (Alfa Aesar 10% Pd)) and Milli-Q water to obtain a total volume similar to the wet volume of the zeolite support. Iridium (III) acetylacetonate (Sigma-Aldrich, 97%) was used as the Ir precursor and was mixed with acetone to prepare the Ir solution. The wet volume of H-SSZ-13 was approximately 0.6 mL/g, close to the total pore volume determined by a N_2 physisorption measurement. The Pt/Pd/Ir solution was dropped slowly in 4 g of H-SSZ-13 zeolite placed in a mortar and after each 8 drops, the mixture was conscientiously ground using a pestle to achieve a homogeneous distribution [75]. After that, the sample was dried overnight at 80 ℃ and subsequently calcined at 600 ℃ for 8 h to obtain the powder catalyst. 1 wt.% Ir/BETA was also prepared following the same synthesis method. A commercial ammonium BETA zeolite (CP814E, Zeolyst) was used that was calcined in an oven at 550 ℃ for 6 h to convert it to its proton form before the impregnation.

3.1.3 Catalyst monolith preparation

The synthesized catalyst powder was dissolved in a solution (50 wt.% ethanol and 50 wt.% Milli-Q water) containing 5 wt.% boehmite binder (Disperal P2, Sasol) as a slurry and washcoated onto a honeycomb monolith (Cordierite, D x L = 1.5 cm * 2.0 cm, 400 cpsi) until the desired dry catalyst loading (300 mg) was reached [76–78]. Then the monolith was subsequently dried in an oven at 80 ℃ overnight and then calcined at 500 ℃ for 2 h. Each washcoated monolith sample was usually prepared in duplicate, with one for testing and the other for backup. Here the catalyst monoliths were prepared and ready for pretreatment before the subsequent activity tests.

3.2 Activity measurements

Catalytic tests were performed with a laboratory-scale flow reactor (synthetic gas bench, SGB), where the monolith was inserted into a horizontal quartz reactor tube (inner diameter: 16 mm) and wrapped in quartz wool to prevent the passage of gases around the outside of the monolith. The inlet gas mixture was regulated by Bronkhorst mass flow controllers (MFCs) and water vapour was produced by a controlled evaporation and mixing system (CEM). The mole fractions of all the gases at the outlet of the reactor were measured and monitored by FTIR (MKS^{TM} multigas 2030) and mass spectrometry (HPR-20 QIC).

3.2.1 Degreening pretreatment

The pretreatments and activity experiments in the flow reactor are presented in **Table 2**. Before the activity tests, a degreening pretreatment was performed to pretreat the catalyst monolith in oxidising and water vapour environments. The de-greening procedure consists of exposing the catalyst monolith to a gas mixture relevant for the application, i.e. lean conditions [79]. The catalyst monolith was ramped up to 550 ℃ at a rate of 5 ℃/min until the temperature was stabilized. Then it was degreened under 10 mol% O_2 in Ar balance at 550 ℃ for 4 h and pretreated using 10 mol% O_2 and 5 mol% H_2O in Ar balance at 500 ℃ for 30 min with a total

flow rate of 1200 NmL/min. The total flow rate was set to obtain a space velocity (20,000 h^{-1}), based on the volume of the monolith (3.54 mL). Ar was used as the inert carrier gas. The feed flow of water was prepared separately by injecting it into 300 NmL/min of Ar before mixing with other feed gases. All calculations of the resulting molar or mass flow rates of gases were based on the ideal gas law. Every monolith sample was degreening pretreated prior to activity testing. In addition, each catalyst powder sample was also degreened prior to any characterisation measurements. The powder samples were placed in a ceramic boat and positioned inside the flow reactor tube to be pretreated under the same conditions.

3.2.2 Reduction pretreatment

To further improve the activity of the catalysts, a reduction pretreatment was used as one strategy that was performed instead of the degreening pretreatment before activity measurements with the monoliths. The reduction conditions are also listed in **Table 2**. It involved flow of 3% H_2 in Ar balance at a total flow of 1200 NmL/min and held at 500 ℃ (5 ℃/min ramp up rate) for 4 h.

3.2.3 Activity test protocol

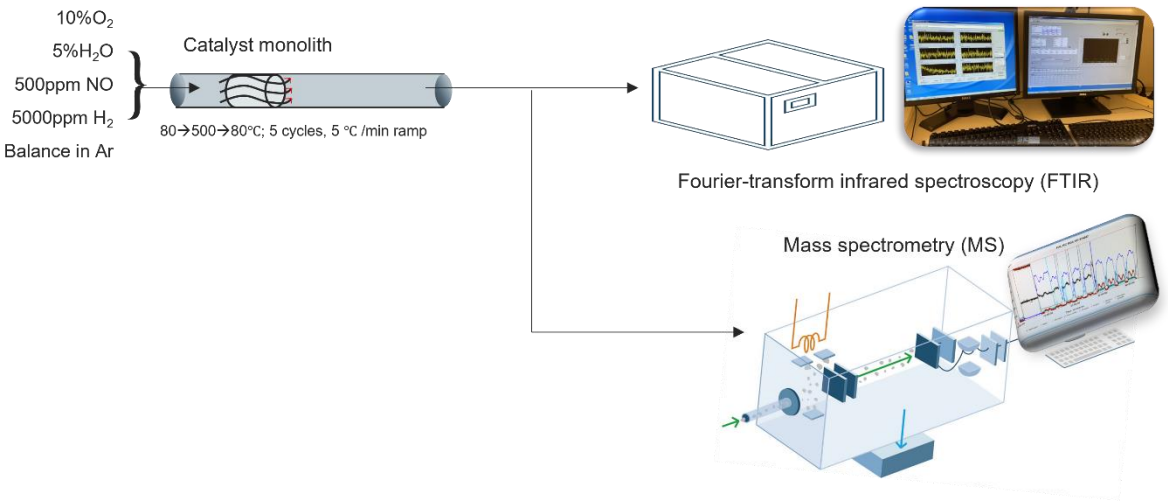

Fig. 6. Schematic overview of the flow reactor set-up.

After the pretreatment, the test cycle involved heating and cooling over a temperature range of 80 to 500 ℃ with a temperature ramp rate of 5 ℃/min. This same test cycle was repeated 5 times to examine any slower changes in the state of the catalyst, caused for example by deactivation or hysteresis effects. In a typical experiment with a molar feed ratio of H_2/NO = 10, the gas composition of the reactivity test was 10% O_2, 5% H_2O, 500 ppm NO, and 5000 ppm of H_2 in Ar balance. Similar tests with H_2/NO ratios of 5 and 15 were also performed by using 2500 and 7500 ppm of H_2, respectively. The outlet gases from the flow reactor were connected to a Fourier-transform infrared spectrometer (FTIR, Multigas2030, MKS) operating at 191 ℃ to analyze the product composition including NO, NO_2, N_2O, NH_3 and H_2O for each catalyst. The analyzer was composed of an IR source, a Michelson interferometer, a gas cell, and a liquid-nitrogen-cooled MCT detector. When the sample is illuminated with IR radiation, a part of the radiation was adsorbed and transmitted. The adsorbed radiation is converted into rotational and/or vibrational energy by the sample molecules. The resulting signal at the

detector is a spectrum, from 4000 cm^{-1} to 600 cm^{-1} with a resolution of 0.5 cm^{-1} and recorded every 3.75 s or 15 s, representing a molecular fingerprint of the gas. The fingerprint means that each specific bond or functional group in a molecule adsorbs IR at a different frequency, resulting in a specific spectrum. The data was analyzed by MKS software suite MF2000 v.10.2 and FTIR-library v.R3. Before the activity tests, a calibration was done using 200/300/400/500 ppm NO, N_2O and NO_2, with and without water. Then, the actual flow rate was compared to the FTIR signal, and a linear relationship was constructed to calculate a calibration factor for subsequent calculations with the reaction data. Since the main-product N_2 cannot be detected by FTIR, the N_2 content was calculated from the mass balance. In order to make direct measurements of the amount of nitrogen and hydrogen as well as other gas components, an additional mass spectrometer (MS) was connected for analysis (**Fig. 6**). In the MS, a sample's gas molecules are converted to rapidly moving positive ions by electron bombardment and charged particles are separated according to their mass to charge ratio, which is also expressed as m/z and then taking a record of the relative abundance of each ion is obtained. A mass spectrum is formed, which shows the spectrum of ion abundance versus mass-to-charge ratio.

Another five-cycle test in the absence of water (dry test) was also performed after the activity tests to study the effect of water on the activity performance of the catalyst. The discussion of the activity test in Section 4 was based on the data of the 4th cycle.

Table 2. The activity test procedure and reaction conditions (GHSV=20,000 h^{-1} (STP)).

Step	Experiment	Conditions
1	Degreening & Pretreatment	(i) 10% O_2 in Ar at 550 ℃ for 4 h (ii) 10% O_2 and 5% H_2O in Ar at 500 ℃ for 30 min
	Reduction pretreatment	3% H_2 in Ar at 500 ℃ for 4 h
2	Cooling	cooling from 500 ℃ to 80 ℃ in Ar (cooling rate: 5 ℃/min) and keep at 80 ℃ for 30 min
3	Test cycle, repeated 5 times	(i) continuous reaction from 80 ℃ to 500 ℃ (heating rate: 5 ℃/min) in the gas mixture of 500 ppm NO, 2500 ppm/5000 ppm/7500 ppm H_2, 10% O_2, 5% H_2O in Ar (ii) keep at 500 ℃ with the same gas mixture for 20 min (iii) continuous reaction from 500 ℃ to 80 ℃ (cooling rate: 5 ℃/min) in the same gas mixture

3.3 Data analysis

As mentioned in Section 3.2, the product gases including NO, N_2O and NO_2 were detected by FTIR. It should be noted that NH_3 was measured, but not detected. The conversion of NO reflects the activity of the catalyst for the reaction. NO conversion and product selectivities were calculated as shown below, neglecting any variations in the total molar flow of the gas due to the reactions, since the NO_x concentrations were very small:

$$NO\ conv.\% = \frac{C_{total} - C_{NO}}{C_{total}} * 100\% \quad (1)$$

$$N_{total} = C_{NO} + C_{NO_2} + 2 * C_{N_2O} \quad (2)$$

$$C_{N_2} = (C_{total} - N_{total})/2 \quad (3)$$

$$C_{NOconvert} = C_{total} - C_{NO} \quad (4)$$

$$N_2\ Sel.\% = \frac{2 * C_{N_2}}{C_{NOconvert}} * 100\% \quad (5)$$

$$NO_2\ Sel.\% = \frac{C_{NO_2}}{C_{NOconvert}} * 100\% \quad (6)$$

$$N_2O\ Sel.\% = \frac{2 * C_{N_2O}}{C_{NOconvert}} * 100\% \quad (7)$$

The total inlet concentration of NO (C_{total}) was 500 ppm. N_2 concentration was in most cases calculated by a mass balance of nitrogen atoms as in Eq.2 and Eq.3 but was also detected by mass spectrometry in some experiments. Selectivity is another important parameter to measure in addition to NO conversion, indicating the amount of converted NO that is converted to each product gas. The selectivity of each product (N_2/N_2O/NO_2) was calculated by Eq.5 – Eq.7. Most of the activity data results in Section 4 are plotted as a function of temperature for the relevant parameters by plotting the NO conversion and each gas product selectivity against the time as the reaction temperature varies.

3.4 Catalyst characterizations

3.4.1 Nitrogen (N_2) physisorption

The textural properties like specific surface area, pore-volume, and pore size of the catalysts were measured by N_2 physisorption at -196 °C using a Tristar 3000 gas analyzer. The supported catalysts (approximately 0.1 g) were degassed in a ½-inch quartz tube at 250 °C for 16 h under N_2 flow to remove moisture. The Brunauer-Emmett-Teller (BET) method in a range of relative pressures p/p_0 from 0.05 to 0.3 was used to calculate the specific surface areas and the t-plot method was used to calculate the microporous volume and external surface areas. In BET surface area analysis, the surface is cooled to the cryogenic temperature for N_2 to dose it stepwise onto the surface in a series of controlled pressure changes. With pressure increases, after the saturation pressure is reached, no further adsorption occurs regardless of any further increase in pressure. After that, the pressure is gradually reduced so that nitrogen is continuously desorbed from the surface which yields the nitrogen-physisorption isotherm. There are five types of adsorption isotherms possible. The BET calculation, by Eq.8 uses the information from the isotherm to determine the surface area of the sample. v is the quantity of nitrogen adsorbed at a given relative pressure (p/p_0) , v_m is the monolayer adsorption

capacity, which is the volume of gas adsorbed at standard temperature and pressure (STP), and c is the BET constant [80].

$$\frac{p/p_0}{v(1-(p/p_0))} = \frac{c-1}{v_m c}\left(\frac{p}{p_0}\right) + \frac{1}{v_m c} \tag{8}$$

However, it should be noticed that the application of the BET equation for determining surface area is limited, especially for zeolite materials which contain micropores and a multi-dimensional pore structure.

3.4.2 X-ray diffraction (XRD)

XRD was used to identify the crystalline phases of the synthesized catalysts in this work. The X-ray diffractograms for all catalysts were obtained using an X-ray powder diffractometer operated at 40 kV and 40 mA (Bruker AXSD8 Advance) with a CuKα monochromatic radiation (λ=1.542A°) source. The samples were scanned in the 2θ range of 5°-80°, with a step size of 0.02° and scan time of 1 second per step. The Bragg equation in **Fig. 7** reflects the relationship between the direction of diffraction lines and the crystal structure [81]. For a particular crystal, only an angle of incidence that satisfies the Bragg's equation can produce an interference enhancement and show diffraction fringes. This is the fundamental meaning of an XRD spectra. When X-rays are irradiated into a sample, the scattered X-rays from the various atoms in the crystal interfere and produce strong X-ray diffraction lines in specific directions. When X-rays are irradiated at different angles to the sample, diffraction occurs at different crystal faces, and the detector will accept the number of diffracted photons reflected from that face, resulting in a spectrum of the angle-intensity relationship.

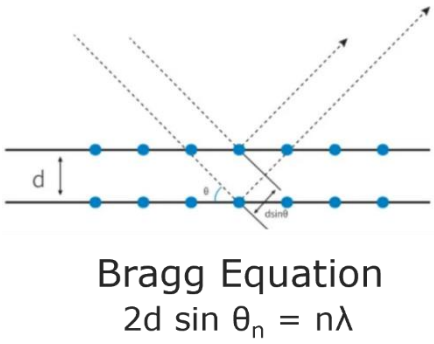

Fig. 7. Bragg equation that could be used for XRD measurement.

3.4.3 Inductively coupled plasma sector field mass spectrometry (ICP-SFMS)

Elemental compositions (Si, Al, O, Pt, Pd, Ir, etc.) of the catalysts were analyzed with inductively coupled plasma sector field mass spectrometry (ICP-SFMS) analysis which was performed by ALS Scandinavia (Luleå, Sweden).

3.4.4 CO chemisorption

CO chemisorption measurements were performed by using an ASAP2020 Chemi Plus instrument (Micromeritics). Around 0.1 g of catalyst powder sample was placed in a U-shape reactor with quartz wool. Before measurement, the sample was degassed in He and underwent

1 h of H_2 reduction at 400 ℃ for pretreatment. After that, the powder sample was evacuated by vacuum to pressures in the range of 100-600 mmHg (at intervals of 25 mmHg) which was used for CO adsorption measurements using the double-isotherm method. The stoichiometry factors (i.e. the number of CO molecules that each active site or metal atom on the catalyst surface binds or adsorbs) used were 1 for Pt, 2 for Pd and 2 for Ir and were used to calculate the dispersion[82–85]. By combining the results of CO chemisorption and ICP, the Pt/Pd/Ir active site densities with different loadings could be calculated. The estimated active site densities with units of μmol. g^{-1}, were calculated by the following equation.

$$Estimated\ site\ density = \frac{W_{washcoat} * 0.95 * Metal\ loading * Dispersion * 10^6}{M * W_{washcoat}}$$

$W_{washcoat}$ – Actual washcoat mass in the monolith;
0.95 – Mass fraction of actual catalyst material (other than binder) in washcoat;
Metal loading – Mass fraction of metal in catalyst from ICP analysis;
Dispersion – from CO chemisorption measurement;
M – Molecular weight of metal.

3.4.5 X-ray photoelectron spectroscopy (XPS)

The chemical state and composition of the catalysts were measured by XPS which was conducted using a PHI5000 VersaProbe III-Scanning XPS MicroprobeTM with an X-ray source of monochromatic Al Kα radiation (Hv=1486.6 eV). Degreened powder samples were taped onto test discs and placed into the chamber to be evacuated for approximately 30 minutes before being sent into the cell. Firstly, test points were selected on the sample and compared with photographs taken while inside the chamber at the beginning, to ensure that the discs did not rotate in any way after entering the chamber. A map scanning was measured to identify all the elements on the sample. This is followed by a detailed scan for a particular metal, which was usually scanned more than 10 times to ensure that the peaks are clear due to the low content of the precious metals on the catalysts. The system was aligned with Au (83.96 eV), Ag (368.21 eV) and Cu (932.62 eV). The measurements were calibrated with the carbon peak (C1s) at 284.8 eV. It should be noted that since the Pt $4f_{5/2}$ and Al 2p lines overlapped, Pt $4f_{7/2}$ was used with the intensity ratio of Pt $4f_{7/2}$: Pt $4f_{5/2}$ = 4:3 and the energy separation between them is around 3.33 eV. The XPSPEAK41 software was employed for the deconvolution of experimental spectra into individual components. Background subtraction and curve fitting were processed by the Shirley model and Gauss-Lorentz functions in the software.

3.4.6 High-resolution transmission electron microscopy (HRTEM)

The morphology of catalyst particles was measured by high-resolution transmission electron microscopy (HRTEM) using an FEI Titan 80-300 microscope equipped with a high-angle annular dark-field (HAADF) detector, with an operating voltage of 300 kV. The average particle size and distribution were calculated by random selection of over 100 particles using ImageJ software.

3.4.7 In-situ diffuse reflectance infrared Fourier transformed spectroscopy (DRIFTS)

In-situ diffuse reflectance infrared Fourier transformed spectroscopy (DRIFTS) spectra were recorded with a Bruker Vertex 70 spectrometer equipped with an MCT detector and scanning

was done at 4 cm^{-1} resolution. A powder sample was placed into a sealed diffuse reflection chamber (Harrick Praying Mantis) equipped with a CaF_2 window. A mass spectrometer (Hiden HR20) was connected to the outlet to the outlet stream to monitor the out-gases.

In-situ DRIFTS was conducted for two studies in **Paper I**. As mentioned before, the degreened catalysts were used for the measurements. Study one was CO adsorption on the Pt/SSZ-13 catalysts to determine the Pt states and thus validate the XPS results, as well as provide the estimation of the stoichiometry factor for CO chemisorption on the Pt [86,87]. The background was recorded at 35 ℃ (catalyst bed temperature) before the measurement. Before each experiment, a pretreatment at 300 ℃ with 100 NmL/min of 10 vol.% O_2 in Ar for 30 min was performed to clean the catalyst surface. Then, a flow of 100 Nml/min containing 1000 ppm of CO/Ar was fed to the cell for 60 min. After that CO feed was cut and the stream composition switched to pure Ar to flush the chamber. The spectrum was recorded 63 times each minute from introducing CO. The second DRIFTS study was to give insight into the reaction mechanism of H_2-SCR by observing different adsorbates on the surface and their changes during the adsorption of NO followed by an introduction of H_2.

For the H_2-SCR mechanism studies, new Pt samples were loaded into the chamber. The detailed protocol is shown in **Table 3**. The background was recorded at 80 ℃ after the pretreatment. Then, three steps were performed, firstly flowing 500 ppm NO for 60 min, flushing with Ar for 30 min, and finally introducing 5000 ppm H_2 for 60 min to investigate the reaction mechanism. In order to exclude the effect of some overlap of the water peaks with the NO adsorption peaks, an additional measurement was performed. This consisted of 5000 ppm H_2 and 5000 ppm O_2 flowing at 80 ℃ for 60 min through the system to form water without any possible NO interference. The water formation spectrum was recorded to compare the water peaks with the peaks in the previous spectrum. Following this, the same three steps (2-4) were repeated to observe the H_2-SCR reaction process. In order to study the different effects of stepwise and simultaneous introduction of reacting gases, the experiment of simultaneous introduction of 500 ppm NO and 5000 ppm H_2 for 60 min was also added. Meanwhile, 5000 ppm O_2 was added afterward to study the O_2 effect on the H_2-SCR reaction.

Table 3. The DRIFTS measurement procedure for H_2-SCR

Step	Experiment	Conditions
	Pretreatment	flowing 10% O_2 in Ar at 300 ℃ for 30 min in total flow of 100 NmL/min
1	Background record	cooling from 300 ℃ to 80 ℃ in Ar (cooling rate: 5 ℃/min); background spectra were recorded
2	NO adsorption	flowing 500 ppm NO in Ar at 80 ℃ for 60 min;
3	Ar	flowing Ar for 30 min
4	H_2-SCR	introducing 5000 ppm H_2 in Ar for 60 min;
	New sample pretreatment	flowing 10% O_2 in Ar at 300 ℃ for 30 min in total flow of 100 NmL/min
5	H_2O formation	cooling from 300 ℃ to 80 ℃ in Ar (cooling rate: 5 ℃/min); flowing 5000 ppm H_2 and 5000 ppm O_2 at 80 ℃ for 60 min;
6	NO adsorption	flowing 500 ppm NO in Ar at 80 ℃ for 60 min;
7	Ar	flowing Ar at 80 ℃ for 30 min
8	H_2-SCR	introducing 5000 ppm H_2 in Ar at 80 ℃ for 60 min;
9	Step 2-4	
10	H_2-SCR (2)	500 ppm NO and 5000 ppm H_2 at 80 ℃ for 60 min;
11	H_2-SCR (3)	500 ppm NO, 5000 ppm H_2 and 5000 ppm O_2 at 80 ℃ for 60 min;

For **Paper II**, DRIFTS measurements were performed to interpret the reaction performance of the three different catalysts (Pt/Pd/Ir). Degreened powder samples were used in this study. After the pretreatment, the background profile was recorded during the cooling process at 200 ℃ and 80 ℃. Then 500 ppm NO was fed to record the NO adsorption onto the catalyst at 80 ℃. The temperature was raised to 200 ℃ and the spectra of NO adsorption were recorded. Then maintaining the temperature at 200 ℃, the feed was switched to 5000 ppm H_2 to observe whether the H_2-SCR occurred. This procedure was repeated for different catalysts, observing differences in peak intensities of adsorbed species, to gain some insights into the reaction mechanism.

4 Results and Discussion

4.1 Characterization results

Three loadings (0.5/1.0/2.0 wt.%) of Pt supported on SSZ-13 zeolite catalysts were prepared for the studies (**Table 4**). For **Paper II**, 1 wt.% Pd/SSZ-13, 1 wt.% Ir/SSZ-13 and 1 wt.% Ir/BETA were prepared. The element contents were determined by ICP-SFMS analysis and the loadings of noble metals Pt and Pd were very close to the nominal values. However, due to the inert nature of iridium, which is difficult to dissolve in various solutions, the ALS company has not established a methodology for measuring the elemental content of Ir, and therefore no ICP data for Ir was obtained. The SiO_2 to Al_2O_3 molar ratio was around 20 for all the samples.

Table 4. Physicochemical properties of Pt, Pd, Ir/SSZ-13 de-greened catalysts.

Nominal loading / wt.%	ICP-SFMS		CO chemisorption			TEM	BET
	Metal /wt.%	SAR (SiO_2/Al_2O_3)	Dispersion/%	Mean particle size/nm	Estimated metal site density/μmol. g^{-1} washcoat	Particle size/nm	Surface area/m^2. g^{-1}
0.5 Pt/SSZ-13	0.51	21.6	18.6	6.1	4.5	5.4	602
1.0 Pt/SSZ-13	1.04	21.8	11.7	9.7	5.7	7.8	616
2.0 Pt/SSZ-13	2.04	19.4	9.9	11.4	9.6	10.1	611
1.0 Pd/SSZ-13	0.98	20.0	64.4	1.7	57.5	/	614
1.0 Ir/SSZ-13	/	/	2.7	53.4	1.3	/	644
1.0 Ir/BETA	/	/	14.3	10.1	7.1	/	524

* Estimated metal site density= $W_{washcoat}$*0.95*loading*dispersion/Mmetal/ $W_{washcoat}$

CO chemisorption measurements were performed to determine the metal dispersion and crystal sizes of the catalysts (**Table 4**). As the Pt loadings increased from 0.5 to 2.0 wt.%, the dispersion of Pt particles decreased from 18.6 to 9.9%. The mean particle sizes determined were 6.1, 9.7 and 11.4 nm for 0.5, 1.0 and 2.0 wt.% of Pt, respectively. The dispersion of Pd for the Pd/SSZ-13 sample was 64.4 % which was considerably higher than for all other samples. The measured particle size from CO chemisorption was only 1.7 nm for Pd/SSZ-13. But for the Ir samples, it is interesting to see that there are so many differences between the two samples loaded with Ir on the SSZ-13 and BETA zeolite. Especially, the 1 wt.% Ir/SSZ-13 catalyst showed a very poor metal dispersion (2.7%), thus very large particles. Therefore, were detailed plots of CO chemisorption explored to examine differences in the behaviors of the samples (**Fig. 8**). Initially, the top curve represents the overall adsorption, encompassing both physisorption and chemisorption on the surface. Subsequently, an evacuation process was implemented to eliminate the physisorbed CO, leading to the repetition of the isotherm and the generation of the lower curve. The variance between these curves signifies the quantity of chemisorbed CO. With the mass of the test powder and the metal loading, the metal dispersion can be calculated by the chemisorbed CO content. Hence, it is observed in **Fig. 8** that there is a low CO chemisorption on the 1 wt.% Ir/SSZ-13 sample surface, which is related to the fact that Ir mostly exists in its oxidised form on the catalyst. However, this situation was improved on the Ir catalysts with BETA as support, which showed significant CO chemisorption. It should be

noted that all catalysts were reduced with hydrogen at 400 ℃ for 1 h in the pretreatment step prior to adsorption. It was demonstrated that the 1 wt.% Ir/SSZ-13 de-greened sample was very difficult to be reduced to its metallic state under these conditions. In addition, the differences in CO chemisorption also reflect the oxidation state of the metals on the surface of the individual catalysts, a property that will be explained in more detail in the subsequent XPS tests. Also, based on the measurements of CO chemisorption, the metal site density could be calculated. It is reasonable that the site densities of the three Pt samples showed an increasing trend in site densities with the loadings. Pd offered a very high active site density due to its high dispersion and very small particle size. For the iridium catalyst, its samples when Ir was loaded on BETA presented a higher site density than that for SSZ-13.

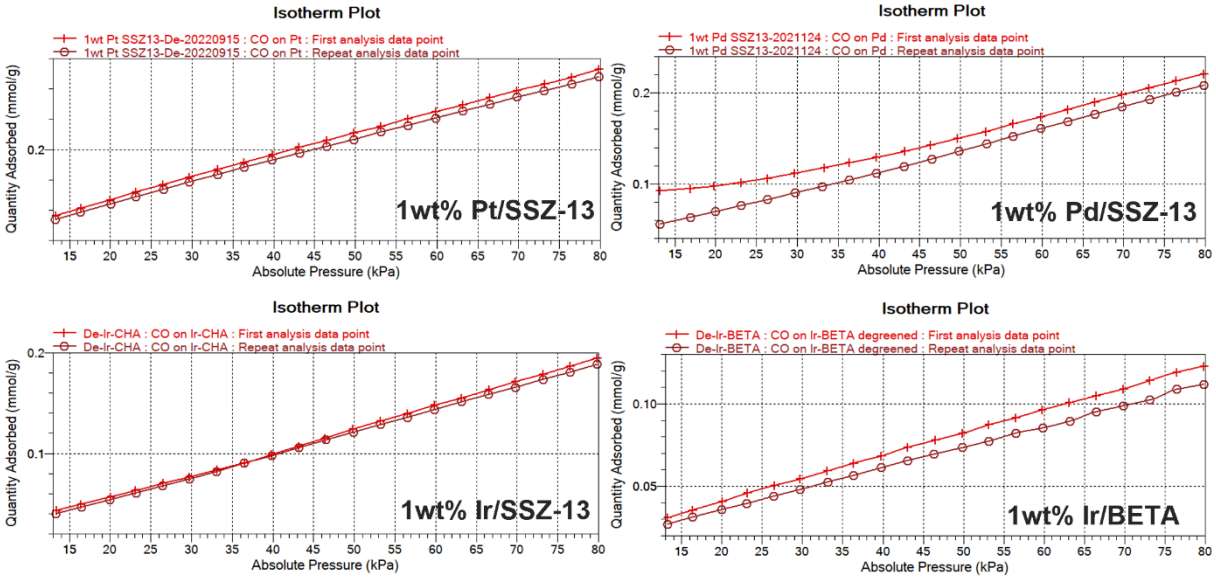

Fig. 8. CO chemisorption plots of degreened 1 wt.% Pt, Pd, Ir/SSZ-13 catalysts and 1 wt.% Ir/BETA catalyst.

The particle sizes of the Pt catalysts were not only determined by CO chemisorption, but also by HRTEM images. The images can be found in **Paper I** and the particle sizes are listed in **Table 4**. The average particle sizes were determined from 100 randomly selected particles in the TEM images. It should be noted that ion-exchanged platinum species are likely present in the catalysts, however, these cannot be observed with the TEM instrument. The average particle sizes increased with Pt loading, corresponding with the CO chemisorption results, from 5.4 nm, 7.8 nm to 10.1 nm for 0.5, 1.0, and 2.0 wt.% Pt/SSZ-13 samples.

According to **Table 4**, samples supported on SSZ-13 zeolite after loading the active metals and degreening pretreatment still showed relatively high surface areas of around 610 m^2g^{-1}. Compared to SSZ-13 zeolite, the BETA zeolite supported Ir sample presented a lower surface area which is related to the different topologies of the zeolites. The BET adsorption and desorption isotherm's linear relationships in **Fig. 9** illustrated that the SSZ-13 gave close to a Type I isotherm in the classification of adsorption isotherms[88] which are given by microporous solids but with large internal surface area. The BETA zeolite yielded a Type II isotherm that is related to a microporous absorbent and it has a hysteresis loop at higher pressure.

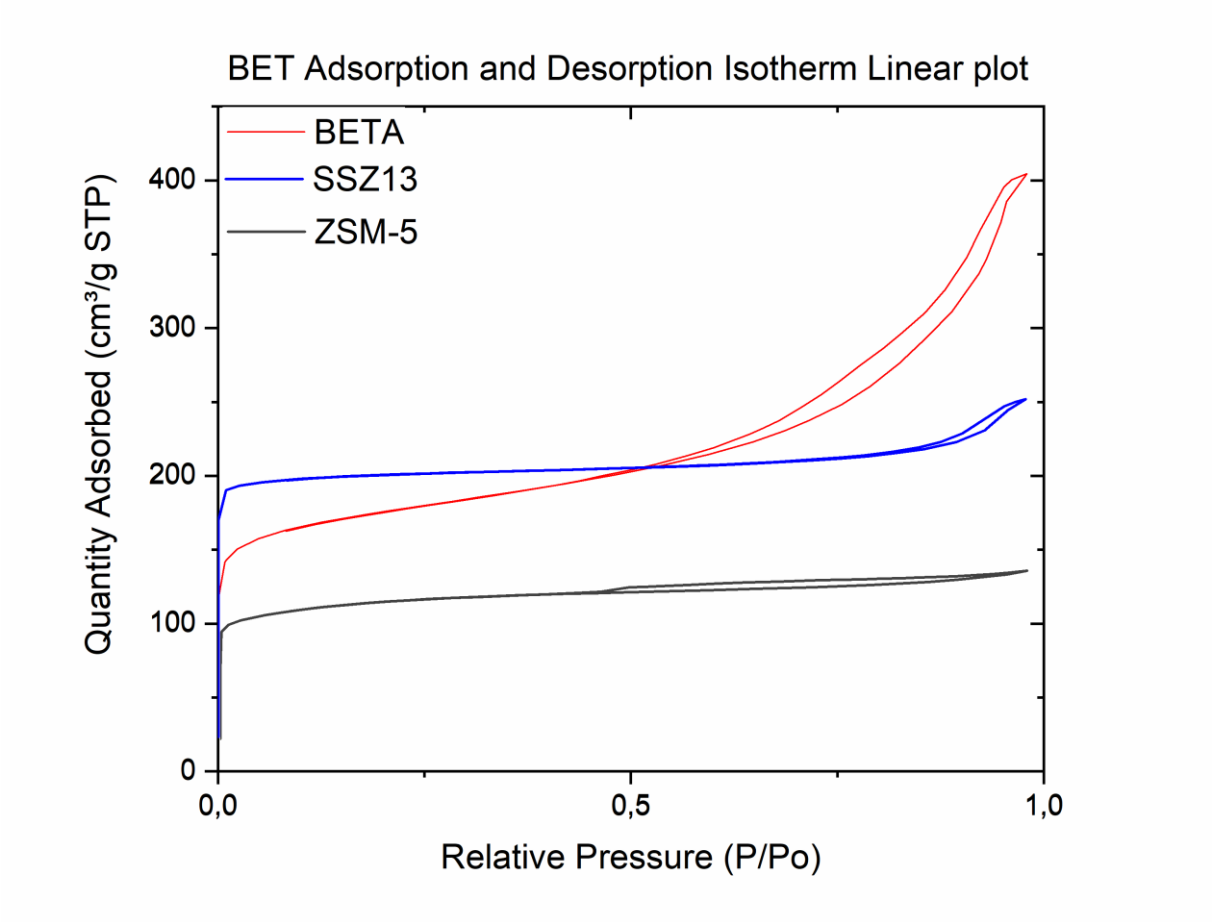

Fig. 9. BET adsorption and desorption isotherm linear plots of BETA, SSZ-13 and ZSM-5 zeolites.

The oxidation states of the samples were measured by XPS. **Fig. 10a** and **Fig. 10b** compare the Pt 4f of degreened Pt samples with 1 wt.% and 2 wt.% loadings. It should be noted that an overlap of the binding energies between Al 2p and Pt 4f makes it difficult to deconvolute the spectrum of Pt 4f, in particular with a low loading of Pt. Only the XPS results for the 1 wt.% Pt/SSZ-13 and 2 wt.% Pt/SSZ-13 samples are presented in **Fig. 10,** since the signals were too weak for the 0.5 wt.% Pt sample. According to the data, the binding energy at 70.6/74.4 eV and 72.5/75.8 eV of the 1 wt.% Pt de-greened sample can be assigned to $4f_{7/2}/4f_{5/2}$ of Pt^0 and Pt^{2+} species, respectively[89,90]. The 1 wt.% Pt sample has a larger amount of metallic Pt (73.7%) than the 2 wt.% Pt sample (24.8%) and a lesser amount of Pt^{2+} at 26.3% compared to 75.2% for the 2 wt.% Pt sample. **Fig. 10c** and **Fig. 10d** show the results for the 1 wt.% Pd/SSZ-13 and 1 wt.% Ir/CHA degreened samples respectively. The binding energies at 335.9/341.2 eV and 338.0/343.4 eV were assigned to $3d_{5/2}/3d_{3/2}$ of Pd^{2+} and Pd^{4+}, respectively [91]. For the Iridium sample, the XPS data is illustrated in **Fig. 10d**, with the binding energies at 62.1/64.9 eV and 63.6/66.6 eV that belongs to $4f_{7/2}/4f_{5/2}$ of the Ir^{3+} and Ir^{4+} species [91]. Comparison of all the degreened samples with 1 wt.% loading revealed that only platinum was present mainly in its metallic state, while Pd and Ir existed only in their oxidised state. Also, iridium was most the oxidised. More detailed XPS data for the Pt catalysts can be found in **Paper I**, while XPS data for Pd and Ir as well as for the samples after their respective reduction pretreatments are shown in **Paper II**.

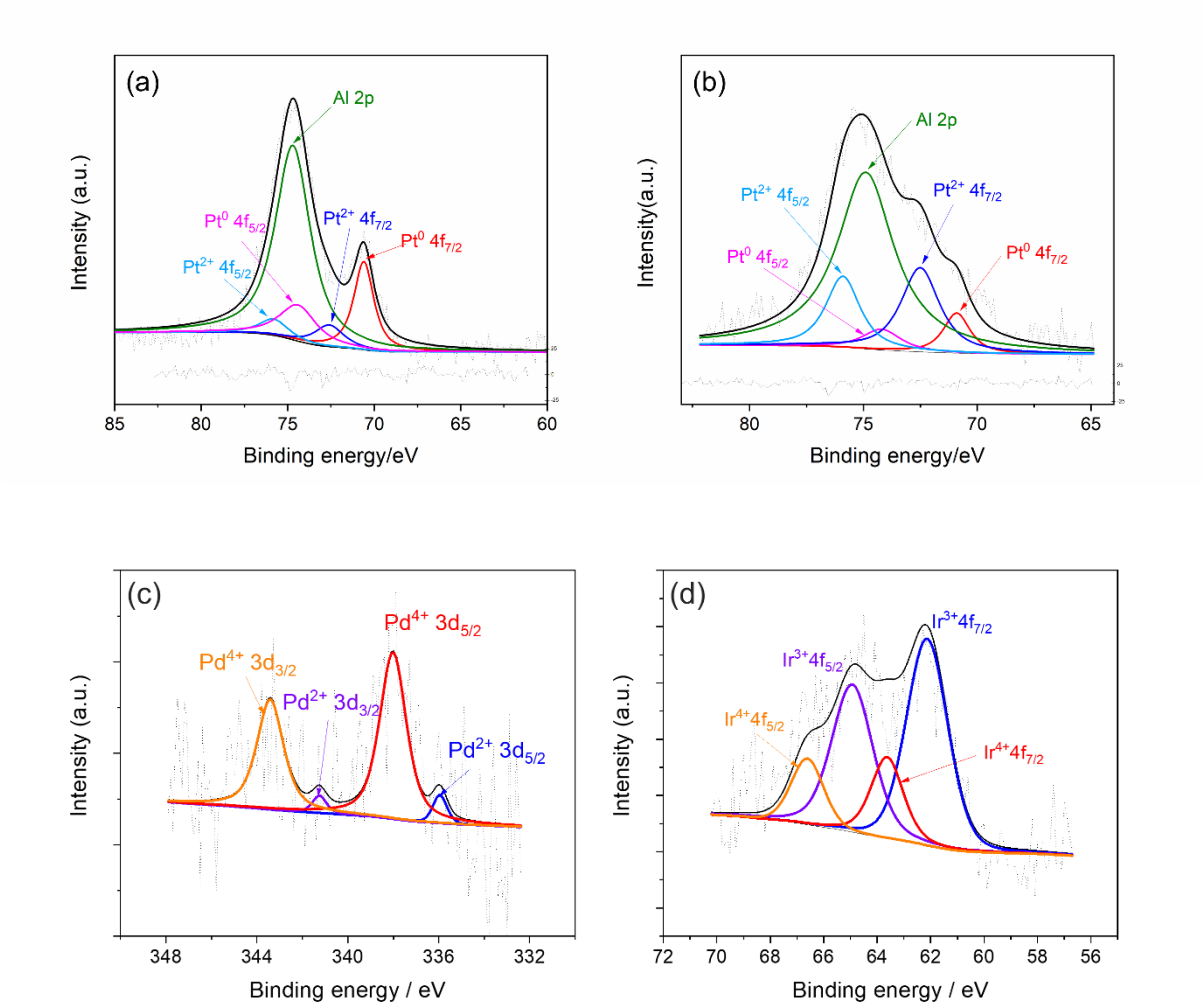

Fig. 10. X-ray photoelectron spectra of (a) 1.0 wt.% Pt/SSZ-13 (b) 2.0 wt.% Pt/SSZ-13 (c) 1 wt.% Pd/SSZ-13 (d) 1 wt.% Ir/SSZ-13 de-greened catalysts.

4.2 Activity tests

4.2.1 Pt catalysts

For the Pt-based catalysts in the H_2-SCR study of the first paper, 0.5/1.0/2.0 wt.% Pt/SSZ-13 were synthesized and measured for their activity performance. The activity test protocol was introduced in Section 3.2.3 and the outlet gas composition was detected by FTIR and MS.

The overall reaction process can be divided into four temperature zones (**Fig. 11a**). In the first region of 80-93 °C, NO concentration decreased and the products N_2 and N_2O increased, indicating H_2-SCR occurred over the Pt/SSZ-13 catalyst. The selectivity for N_2O is higher than N_2 at this stage (black and red curves). The mechanism of N_2O production has been mentioned in Section 2.1.1 according to the literature[30]. In the temperature range 97 °C to 150 °C, it is noticed that the N_2O production starts to drop dramatically and the N_2 first increased and then decreased. To interpret this observation, N_2O reduction by H_2 was tested on the 1 wt.% Pt sample which showed that N_2O could not be reduced to N_2 on the Pt/SSZ-13 catalyst (**Fig.11b**). Hence, we considered that it is due to the H_2-SCR preferring to produce N_2 than N_2O in this temperature range. Also, as the temperature rises, the H_2 oxidation was enhanced which limited the availability of H_2 which resulted in suppressed N_2 production. Eventually, hydrogen is further consumed with temperature resulting in NO oxidation to NO_2 at higher temperatures gradually becoming the dominant reaction, while the products N_2 and N_2O of H_2-SCR still gradually decreased. Although, N_2 decreased somewhat more slowly than N_2O. Finally, at the highest temperatures, the NO oxidation was suppressed due to thermodynamic equilibrium. A more detailed description can be found in **Paper I**.

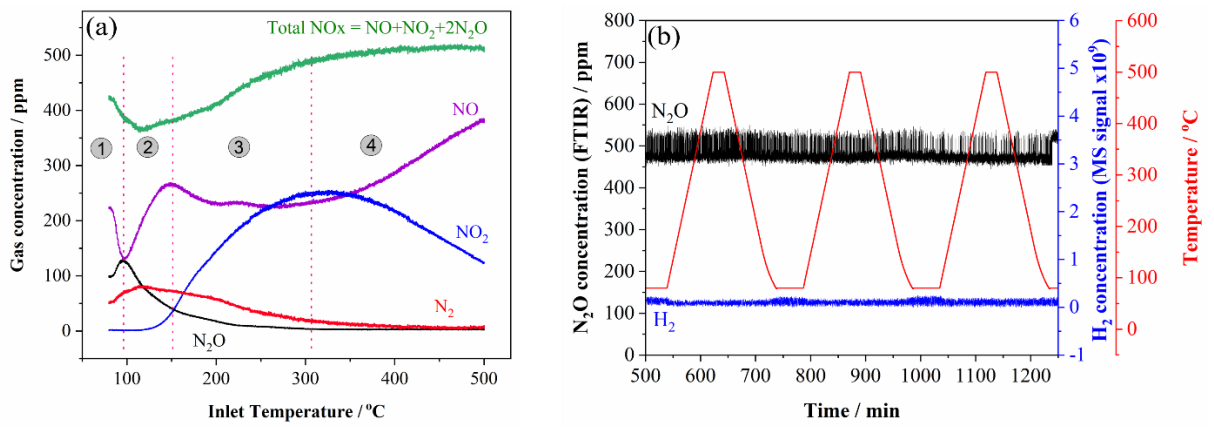

Fig. 11. (a) NO_x and N_2 concentration of H_2-SCR reaction on 2 wt.% Pt/SSZ-13 catalyst (b) The activity results of N_2O reduction by H_2 on 1 wt.% Pt/SSZ-13 catalyst (GHSV=20,000 h^{-1} (STP); gas inlet: 10% O_2, 5% H_2O, 500 ppm NO/N_2O, 5000 ppm H_2 balanced in Ar; T: 80-500 °C; heating rate: 5 °C/min).

After an initial exploration of the complex reaction process, the effect of reaction conditions was further investigated, including the feed ratio of H_2/NO, the metal loading of Pt, and wet and dry environments. As shown in **Fig.12**, in the absence of hydrogen, only NO oxidation at high temperatures occurred. The peak of H_2-SCR conversion at low temperatures appeared after the introduction of hydrogen. A greater H_2 proportion favored the target product N_2 which is due to the higher active H atom density on the Pt centers promoting the complete reduction of NO to N_2. NO oxidation became dominant at high temperatures because H_2 is rapidly consumed by its combustion (**Paper I**). Interestingly, H_2 cannot only support N_2 reduction but also assists

the NO oxidation at lower temperatures. One possible reason is that the larger H_2 oxidation with higher H_2 concentration resulted in increased reaction heat and thereby an increased temperature of the catalyst surface.

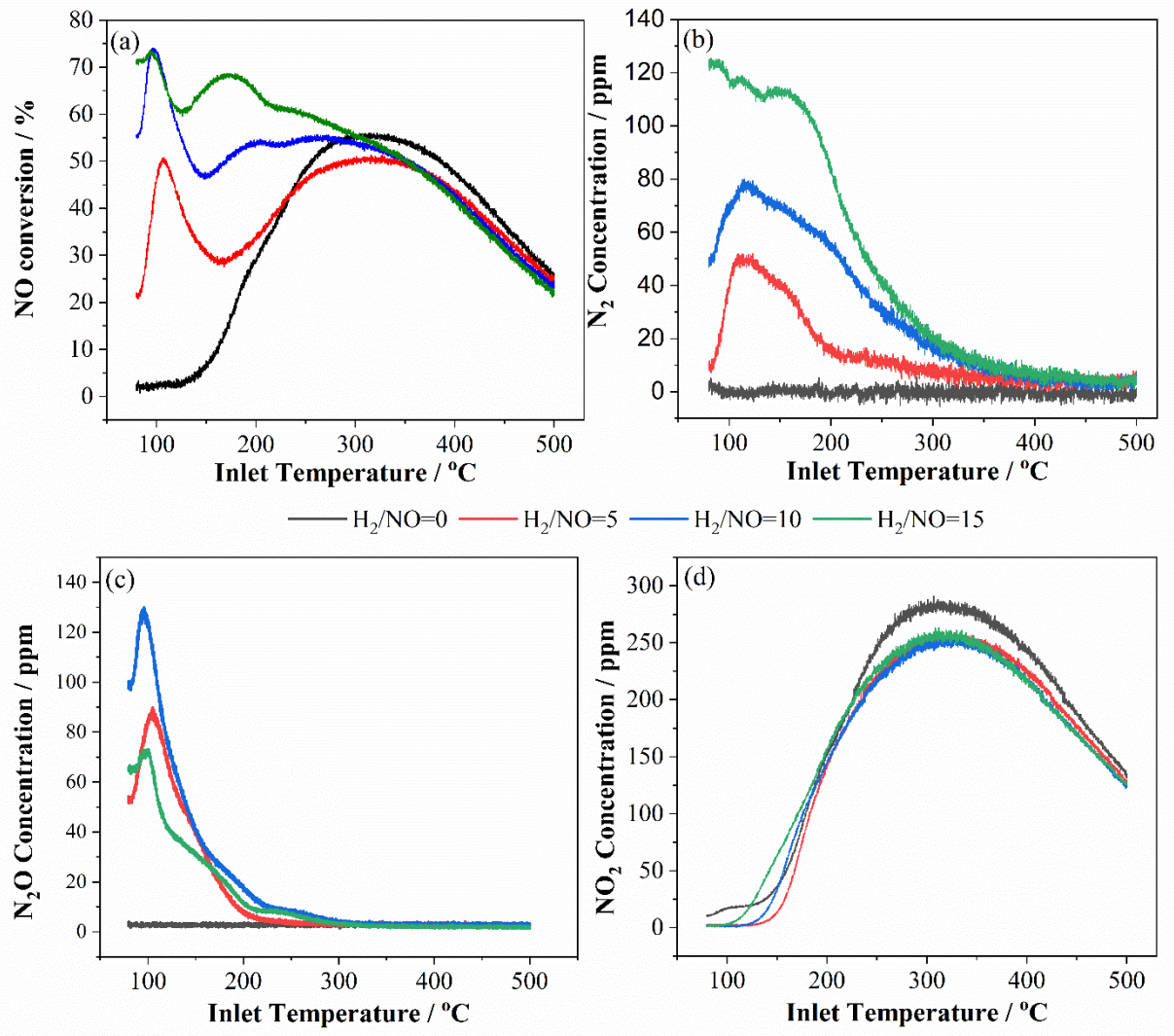

Fig. 12. Comparison of the effect of different H_2/NO ratios on 2 wt.% Pt/SSZ-13 catalyst, where (a) shows the conversion, and the concentration profiles are shown in (b) N_2 (c) N_2O (d) NO_2 (GHSV=20,000 h^{-1} (STP); gas inlet: 10% O_2, 5% H_2O, 500 ppm NO, 2500/5000/7500 ppm H_2 balanced in Ar; T: 80-500 °C; heating rate: 5 °C/min).

It was found that the Pt loading had a significant effect on the activity performance (**Fig. 13**). **Table 5** shows that the 2 wt.% Pt sample had approximately twice the active site density compared to the 0.5 wt.% Pt sample. However, it was not the case that a higher content of active centers was more beneficial for H_2-SCR. On the contrary, the highest conversion for NO oxidation was achieved on the 2 wt.% Pt sample. Also, H_2 was more oxidized on 2 wt.% Pt sample that led to the lowest NO reduction conversion at low temperatures. From comparison of the selectivity for each product, it was found that 0.5 wt.% Pt had the highest N_2 selectivity, reaching 75% at 167 °C. Through various characterizations, it was demonstrated that particle size, dispersion, metallic states, etc. were responsible for the highest NO reduction and highest N_2 selectivity of the 0.5 wt.% sample. However, it is also important to recognize that there were differences in the H_2 conversion over the catalysts with varying Pt loading which influenced the H_2 availability in the monoliths at varying temperatures. For example, with the 0.5 wt.%

sample, the H_2 conversion increased more slowly with temperature, which maintained a higher H_2 concentration at higher temperatures which is beneficial for H_2-SCR.

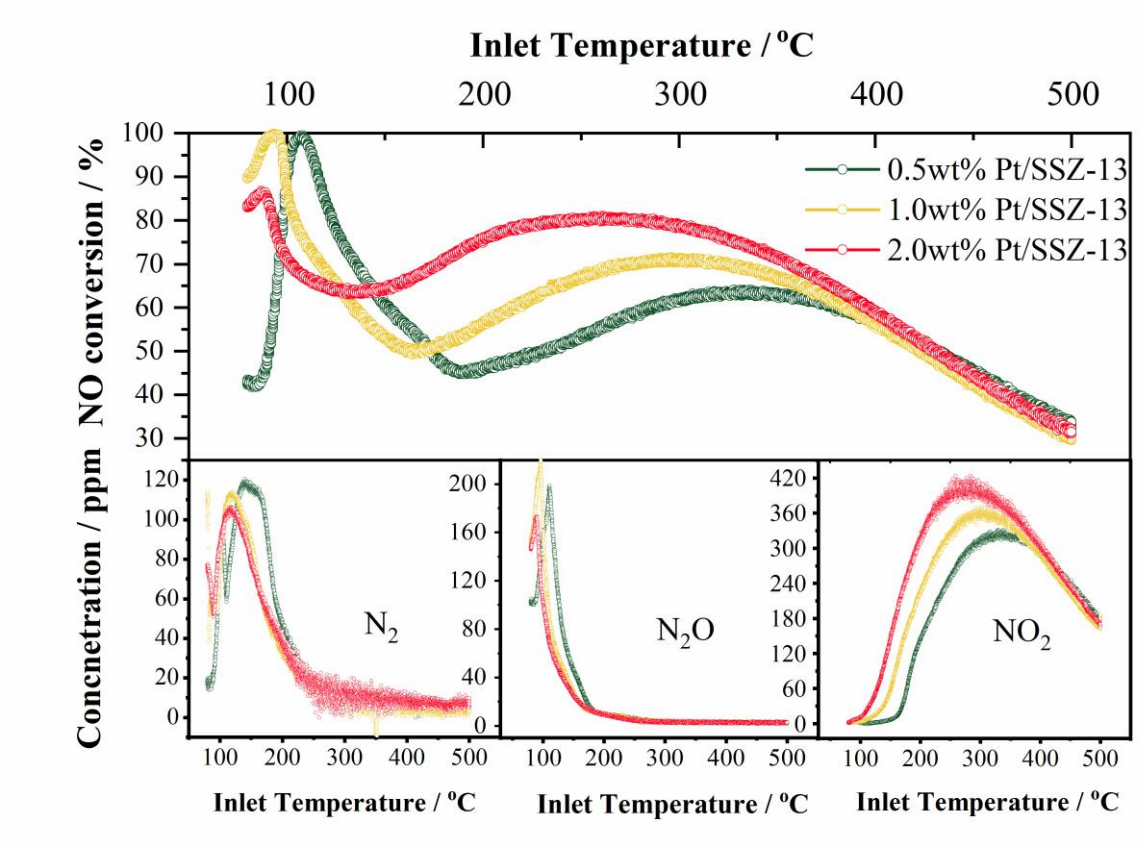

Fig. 13. Comparison of NO conversion and $N_2/N_2O/NO_2$ concentration profiles on Pt/SSZ-13 catalysts with different Pt loadings (GHSV=20,000 h^{-1} (STP); gas inlet:10% O_2, 5% H_2O, 500 ppm NO, 5000 ppm H_2 balanced in Ar; T: 80-500 °C; heating rate: 5 °C/min).

The influence of water is important to consider, especially for the aftertreatment of hydrogen internal combustion engines, where large quantities of water would be present in the exhaust gas. **Fig.14** compares the activity of the 1 wt.% Pt sample in the presence and absence of water. Water had a significant inhibition effect at low temperature on H_2-SCR over the Pt catalyst which is due to the competitive adsorption of water on the active sites. The N_2 signal from MS measurements was observed to be higher in the absence of water than in the presence of water. Not only N_2 was affected, the N_2O formation was also less pronounced when the system was without water addition, which also indicated that N_2 selectivity during H_2-SCR improved under dry conditions. At higher temperatures, the influence of water was less because of greater water desorption from active sites that reduced its inhibiting effect.

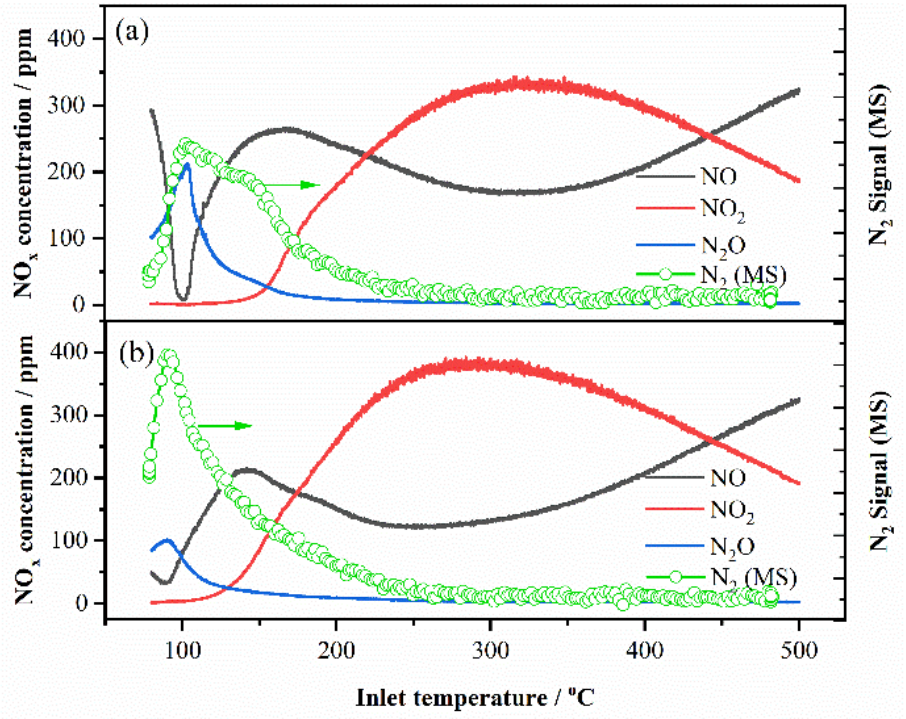

Fig. 14. Comparison of $NO/NO_2/N_2$ concentration from FITR and N_2 Signal from MS of 1 wt.% Pt/SSZ-13 catalyst (a) with H_2O and (b) without H_2O (GHSV=20,000 h^{-1} (STP); gas inlet: 10% O_2, 0%/5% H_2O, 500 ppm NO, 5000 ppm H_2 balanced in Ar; T: 80-500 °C; heating rate: 5 °C/min).

4.2.2 Pd and Ir catalysts

1 wt.% Pd/SSZ-13 and 1 wt.% Ir/SSZ-13 were measured following the same procedure to compare their activity performance with 1 wt.% Pt/SSZ-13 catalyst (**Fig.15a**). It was found that the three catalysts have their different working temperature intervals (low-medium-high), respectively. This is also the key point in **Paper II**. As mentioned in Section 4.2.1, H_2-SCR only occurs at low temperature over the Pt catalyst, whereas H_2-SCR on the Pd catalyst has a higher and wider reaction temperature interval, although NO conversion is about 20% of that of Pt. The N_2 selectivity on Pd was maintained at 80% in the medium temperature region, but the Pt catalyst only had a maximum selectivity of 70% at one temperature point, 150 °C (**Fig.16**). The Ir catalyst had the highest working temperature interval (>250 °C), but also the lowest NO conversion. Surprisingly, the N_2 selectivity was however very high during its catalytic temperature window. This specific high-temperature property of Ir is important for the H_2-ICE since the exhaust gases could have high and wide temperature profiles. Since each catalyst exhibited a distinct working temperature window, an attempt was made to examine the activity of a combination of the three catalysts positioned sequentially in order of Ir/SSZ-13-Pd/SSZ-13-Pt/SSZ-13, under the same flow and feed gas composition. The Pt sample was positioned furthest downstream to avoid premature consumption of H_2 by its extraordinary oxidation activity. **Fig.15b** shows that with this arrangement, nitrogen generation exhibited two distinct peaks in the low-medium-high temperature zones, although the last caused by Ir is hardly visible. This concept shows large potential, however, the activity for the iridium catalysts needs improvement.

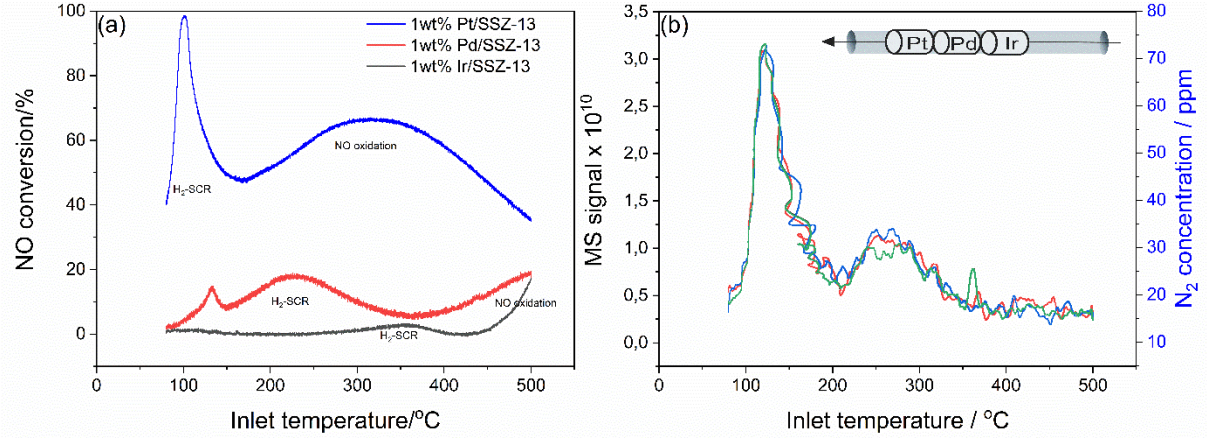

Fig. 15. (a) NO conversion of de-greened 1 wt.% Pt/SSZ-13, 1 wt.% Pd/SSZ-13 and 1 wt.% Ir/SSZ-13 de-greened samples. (b) MS signals of N_2 generation and calibrated concentration (3 cycles) from the catalyst series: Ir/SSZ-13-Pd/SSZ-13-Pt/SSZ-13.

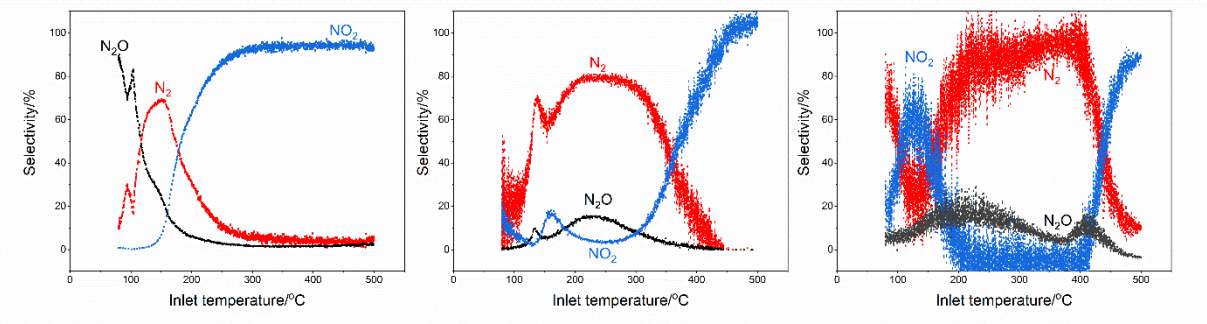

Fig. 16. Selectivity of de-greened 1 wt.% Pt/CHA, 1 wt.% Pd/CHA and 1 wt.% Ir/CHA. N_2 is determined by mass balance using FTIR data.

Two strategies were used to improve the activity of the Ir catalyst. As discussed in Section 4.1, XPS measurement results indicated the Pd and Ir catalysts were essentially completely in their oxidized states. The first strategy was a reduction pretreatment of the Ir catalyst, for which the conditions are outlined in Section 3.2.2. Ir was also loaded onto BETA zeolite instead of SSZ-13 zeolite via the same incipient wet impregnation method as a second strategy to further improve the reactivity of iridium. According to **Fig. 17**, with an H_2 pretreatment, the reactivities were improved for both SSZ-13 and BETA supports. Notably, the H_2-pretreated Ir/BETA catalyst showed a doubled maximum N_2 generation, compared to a more moderate increase for the H_2-pretreated Ir/SSZ-13 (max. 30 ppm vs. 15 ppm). However, the working temperature window for the H_2-pretreated Ir/BETA shifted to lower temperatures. XPS results (**Paper II**) revealed that after H_2-pretreatment, Ir was present in a more reduced form both on BETA zeolite and SSZ-13 zeolite, which may be one of the important reasons for the increase in activity. Comparison of the XPS results of Ir/BETA and Ir/SSZ-13 showed that a larger fraction of the metal was in more reduced states on Ir/BETA, which explains the shift of its nitrogen formation to a lower temperature.

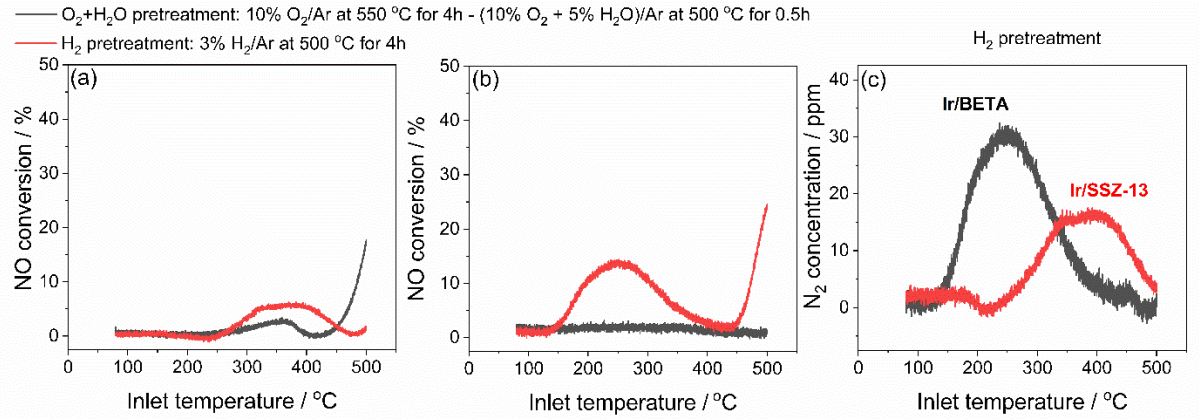

Fig. 17. (a) NO conversion of degreened and reduced 1 wt.% Ir/SSZ-13 (b) NO conversion of degreened and reduced 1 wt.% Ir/BETA (c) N_2 concentration of reduced 1 wt.% Ir/SSZ-13 and 1 wt.% Ir/BETA catalysts.

4.3 DRIFTS studies

4.3.1 CO adsorption

CO adsorption was performed in DRIFTS measurements to confirm the XPS results for the redox states of platinum in Pt/SSZ-13 catalysts. The different CO adsorption peaks represent different species of adsorbed platinum, namely the metallic, oxidised and partially oxidised states of Pt. The results demonstrate that after the degreening pretreatment, the 0.5 wt.% Pt/SSZ-13 had more Pt in its metallic state and the least Pt in its oxidised state, which supports the XPS results.

4.3.2 H_2-SCR on Pt/SSZ-13 catalyst

In **Paper I**, DRIFTS measurements of H_2-SCR on degreened 1 wt.% Pt/SSZ-13 at 80 °C was carried out, which was divided into three main steps: NO adsorption, inert flushing and H_2 exposure. In the first two steps it was found that NO was absorbed on the surfaces of Pt and the support in different forms and that after cutting off the NO gas, the NO_x adsorbed started to desorb due to weaker adsorption. The H_2-SCR reaction occurred after the addition of hydrogen, which produced large peaks at high wavenumbers representing the water product adsorption, as well as a multitude of other newly generated peaks. However, since the water peaks overlapped with the NO adsorption peaks, new experiments were designed in order to exclude the interfering effects of water when defining each IR peak.

The H_2-oxidation reaction was carried out by passing only hydrogen and oxygen over the catalyst, thus determining the location of each peak of water on the catalyst. Then NO adsorption and H_2-SCR were performed to compare with it to exclude the overlapping effects of water. Finally, the differences between the sequential and simultaneous passage of NO and H_2 and the peaks in the presence of excess oxygen were investigated. The specific experiments and their results are explained in detail in **Paper I**. The main conclusions included the following i) Nitrosyl species weakly adsorbed on the acidic sites of the zeolite can be easily removed. ii) H_2 was absorbed on Pt active sites rather than the support surface and was activated to interact with NO that was also absorbed on the Pt surface. iii) NH_4^+ ions were formed on the surface and can play a role as a reaction intermediate to assist in the reduction of NO. iv) The reaction

occurs rapidly when NO and H_2 enter simultaneously, where the form of adsorption of NO on the surface changed. v) The addition of O_2 to an NO+H_2 mixture generates more nitrite (NO_2^-) species on the catalyst.

4.3.3 NO adsorption profiles and H_2-SCR on Pt, Pd, Ir/SSZ-13 catalysts

DRIFT spectra were examined with de-greened 1 wt.% Pt/SSZ-13, Pd/SSZ-13 and Ir/SSZ-13 catalysts to study differences in the mechanism with the catalysts regarding two steps – NO adsorption and H_2-NO reaction. The main focus was to compare differences in NO adsorption behavior and the H_2-NO reaction behavior of the three catalysts at 80 and 200 ℃. The results demonstrated that the de-greened Ir catalyst had the strongest NO adsorption and thus did not catalyse the H_2-NO reaction at 200 ℃ due to the strong NO adsorption as well as its inert nature. After reduction pretreatment, NO adsorption on the surface of Ir at 200 ℃ is weakened, which contributes to the subsequently improved reaction activity. In addition, the Pd catalyst surface has a different NO adsorption than the other two other catalysts, where a larger fraction of Pd existed as exchanged Pd ions. A more detailed explanation can be found in **Paper II**.

5 Conclusions

The main objective of this thesis project is to develop highly efficient H_2-SCR catalysts with high N_2 selectivity. On this basis, understanding their water resistance and suitable operating temperature ranges are also important.

Catalysts with Pt as the active centre and SSZ-13 as the carrier were investigated in **Paper I**. Firstly, it was discussed that the total reaction process can be divided into four regions according to temperature, with the H_2-SCR reaction occurring predominantly with high NO conversion at low temperatures, but with the production of the by-product N_2O being initially more abundant than N_2 and gradually decreasing. At high temperatures, only NO oxidation to NO_2 occurs as the hydrogen combustion reaction consumes most of the hydrogen. After examining various reaction conditions, it was found that the H_2 content contributed to increased N_2 selectivity and also caused more exothermic hydrogen oxidation, promoting earlier NO oxidation. When studying the effect of Pt loading, it was found that lower loading was more favorable for N_2 selectivity. This is due to multiple factors. On the one hand, fewer active centres lower rate of the competing reaction H_2 combustion which allows better penetration of H_2 into the monolith and maintains a higher H_2/NO ratio that is favorable for N_2 selectivity. On the other hand, the lowest loading (0.5 wt.% Pt/SSZ-13) was found to have the highest dispersion and the smallest particle size from various characterization data, and the XPS and CO adsorption data together indicated that it had the highest portion of Pt in the metallic state. In addition, water had a significant inhibitory effect on the reaction at low temperatures, mainly in the form of a large reduction in N_2 generation compared to anhydrous conditions. Finally, the mechanism of the reaction was initially explored using DRIFTS. In order to exclude the interference of water adsorption peaks on NO adsorption, a separate reaction of H_2-O_2 on the surface of the Pt catalyst was designed to compare with results from NO-H_2 reaction. In addition, control experiments with stepwise and simultaneous feed of NO and H_2 as well as experiments on the effect of excess oxygen participation in the reaction were also designed. It was found that when H_2 was introduced on an NO saturated sample at 80 ℃, water formation was observed showing that the SCR reaction was started. H_2 is absorbed on the surface of Pt active sites and is activated to interact with nitrates. Meanwhile, NH_4^+ ions were formed during the reaction and played a role as reaction intermediates to assist in the reduction of NO. Simultaneous feed of NO and H_2 induces a faster reaction than sequential feed and influences the binding of surface species, especially NO. The introduction of O_2 to an NO+H_2 mixture generates more nitrite (NO_2^-) species on the catalyst.

In **Paper II** the main focus was on extending the temperature range of the reaction by combining three different active metals (Pt, Pd, Ir). The activity data demonstrated that 1 wt.% Pt/SSZ-13, 1 wt.% Pd/SSZ-13 and 1 wt.% Ir/SSZ-13 acted to catalyze N_2 formation in the low (80-250 ℃), medium (110-390 ℃) and high temperature ranges (245-470 ℃), respectively. In contrast, the selectivity for N_2 progressively increased with temperature. This is related to their own catalytic reaction activities as well as the redox properties of the metals. Their inherent catalytic activity also greatly affects the competing reaction-hydrogen combustion. In other words, Pt with high activity is also more active for the H_2 oxidation which depletes H_2 in large

quantities at an early stage, leaving no possibilities to reduce NO at high temperatures. Whereas XPS analysis showed that only de-greened Pt/SSZ-13 catalyst remains in mostly its metallic state, Pd and Ir exist only in their oxidised states. Thereafter, in response to the lower catalytic activity of iridium, the NO conversion was successfully improved by reduction pretreatment and by loading onto a BETA zeolite support. While a DRIFTS study of the reaction mechanism indicated that de-greened 1 wt.% Ir/SSZ-13 had a stronger NO adsorption than other catalysts. H_2-SCR did not occur at 200 ℃ due to the stronger NO adsorption and lower catalytic activity of the Ir sample. However, after reduction pretreatment, NO adsorption on the surface of Ir at 200 ℃ was weakened and the reaction successfully occurred.

6 Future Work

In **Paper I**, the Pt catalysts were mainly investigated, and it was found that although their activity was high, N_2O by-product formation was high, and the temperature interval of Pt catalysts is narrow. In contrast, catalysts with two other active centres (Pd, Ir) were explored in **Paper II**, and it was found that Pd/SSZ-13 had a higher and wider temperature active interval than Pt, while N_2 selectivity was maintained at about 80%. The catalytic activity of Pd is higher than that of Ir, so it is believed that there is potential for continued development of palladium catalysts. For the development of palladium catalysts, the primary need is to improve their NO conversion. Factors that can be considered to achieve improvements include support and additive effects. Another important factor is the effect of water. As emphasized in Section 4.2.1, the exhaust gases of hydrogen internal combustion engines contain a large amount of water, so good water resistance is particularly important for H_2-SCR catalysts. Pd catalysts have been found to have much better water resistance than Pt catalysts (experiments not shown in this thesis), and an investigation of water resistance under higher water content as well as an in-depth study of specific mechanistic effects of water are of importance.

The results from **Paper II** revealed that the redox state of the metals has a large effect on the reaction and is correlated with temperature. So, the next step will be to observe and track the real-time metal redox state changes during the reaction process and carry out a deeper investigation of the dynamic reaction mechanism. In such a study water could also be introduced to create different gas environments and observe its effect on the metal redox states during in-situ measurements.

7 References

(1) https://h2tools.org/bestpractices/hydrogen-compared-other-fuels.

(2) Gillingham K. Hydrogen internal combustion engine vehicles: a prudent intermediate step or a step in the wrong direction. Stanford University: Stanford, CA, USA. **2007**.

(3) Verhelst, S.; Thomas, W. Hydrogen-fueled internal combustion engines. *Progress in energy and combustion science* **2009**, *35* (6), 490-527.

(4) Stępień, Zbigniew. A comprehensive overview of hydrogen-fueled internal combustion engines: Achievements and future challenges. *Energies* **2021**, *14* (20), 6504.

(5) Boretti, A. Hydrogen Internal Combustion Engines to 2030. *Int J Hydrogen Energy* **2020**, *45* (43), 23692–23703.

(6) Swain, M.R.; Pappas, J.M.; Adt, R.R., Escher, W.J. Hydrogen-fueled automotive engine experimental testing to provide an initial design-data base. *SAE Technical Paper*. No. 810350, **1981**.

(7) https://www.epa.gov/no2-pollution/basic-information-about-no2#Effects.

(8) Vestreng, V.; Ntziachristos, L.; Semb, A.; Reis, S.; Isaksen, I.S.; Tarrason, L. Evolution of NO x emissions in Europe with focus on road transport control measures. *Atmospheric Chemistry and Physics* **2009**, *9* (4), 1503-1520.

(9) https://www3.epa.gov/region1/airquality/nox.html.

(10) https://www.eea.europa.eu/data-and-maps/indicators/eea-32-nitrogen-oxides-nox-emissions-1/assessment.2010-08-19.0140149032-3.

(11) https://www.naturvardsverket.se/data-och-statistik/luft/utslapp/utslapp-av-kvaveoxider-till-luft/).

(12) Boningari, T.; Smirniotis, P.G. Impact of nitrogen oxides on the environment and human health: Mn-based materials for the NO_x abatement. *Current Opinion in Chemical Engineering* **2016**, *13*, 133-141.

(13) Cohn, Johann GE; Duane R. Steele; Holger C. Andersen. Method of selectively removing oxides of nitrogen from oxygen-containing gases. U.S. 2,975,025. **1961**.

(14) Cobb, D.; Glatch, L.; Ruud, J.; Snyder, S. Application of Selective Catalytic Reduction (SCR) Technology for NO_x Reduction from Refinery Combustion Sources. *Environmental Progress* **1991**, *10* (1), 49–59.

(15) Hosseini, S. E.; Butler, B. An Overview of Development and Challenges in Hydrogen Powered Vehicles. *International Journal of Green Energy* **2020**, *17* (1), 13-37.

(16) Yin, C.; Wang, L.; Rivillon, S.; Shih, A. J.; Yang, R. T. SCR of Nitric Oxide by Hydrogen over Pd and Ir Based Catalysts with Different Supports. *Catal Letters* **2015**, *145* (7), 1491–1499.

(17) Hecker, W. C.; Bell, A. T. Reduction of NO by H_2 over silica-supported rhodium: Infrared and kinetic studies. *Journal of Catalysis* **1985**, *92* (2), 247-259.

(18) Ueda, A.; Nakao, T.; Azuma, M.; Kobayashi, T. Two conversion maxima at 373 and 573 K in the reduction of nitrogen monoxide with hydrogen over Pd/TiO_2 catalyst. *Catalysis Today* **1998**, *45* (1-4), 135-138.

(19) Hu, Z.; Yang, R. T. 110th Anniversary: Recent Progress and Future Challenges in Selective Catalytic Reduction of NO by H_2 in the Presence of O_2. *Ind Eng Chem Res* **2019**, *58* (24), 10140–10153.

(20) Chorkendorff, I.; Niemantsverdriet, J. W. *Concepts of Modern Catalysis and Kinetics*; Wiley, **2003**.

(21) Costa, C. N.; Efstathiou, A. M. Low-Temperature H_2-SCR of NO on a Novel Pt/MgO-CeO_2 Catalyst. *Appl Catal B* **2007**, *72* (3–4), 240–252.

(22) Frank, B.; Emig, G.; Renken, A. Kinetics and mechanism of the reduction of nitric oxides by H_2 under lean-burn conditions on a $Pt–Mo–Co/\alpha$-Al_2O_3 catalyst. *Applied Catalysis B: Environmental* **1998**, *19* (1), 45-57.

(23) Giordanino, F.; Borfecchia, E.; Lomachenko, K. A.; Lazzarini, A.; Agostini, G.; Gallo, E.; Soldatov, A. V.; Beato, P.; Bordiga, S.; Lamberti, C. Interaction of NH_3 with Cu-SSZ-13 Catalyst: A Complementary FTIR, XANES, and XES Study. *Journal of Physical Chemistry Letters* **2014**, *5* (9), 1552–1559.

(24) Hecker, W. C.; Bell, A. T. Reduction of NO by H_2 over silica-supported rhodium: Infrared and kinetic studies. *Journal of Catalysis* **1985**, *92* (2), 247-259.

(25) Burch, R.; Watling, T. C. Adsorbate-assisted NO decomposition in NO reduction by C_3H_6 over Pt/Al_2O_3 catalysts under lean-burn conditions. *Catalysis letters* **1996**, 37, 51-55.

(26) Papp, H.; Sabde, D. P. An Investigation on the Mechanism of NO Decomposition over Rh/SiO_2 Catalysts in Presence of Pulse Injected H_2. *Appl Catal B* **2005**, *60* (1–2), 65–71.

(27) Zhou, S.; Varughese, B.; Eichhorn, B.; Jackson, G.; McIlwrath, K. Pt-Cu Core-Shell and Alloy Nanoparticles for Heterogeneous NO_x Reduction: Anomalous Stability and Reactivity of a Core-Shell Nanostructure. *Angewandte Chemie* **2005**, *117* (29), 4615–4619.

(28) Shibata, J.; Hashimoto, M.; Shimizu, K. I.; Yoshida, H.; Hattori, T.; Satsuma, A. Factors Controlling Activity and Selectivity for SCR of NO by Hydrogen over Supported Platinum Catalysts. *Journal of Physical Chemistry B* **2004**, *108* (47), 18327–18335.

(29) Zemlyanov, D.Y.; Smirnov, M.Y.; Gorodetskii, V.V.; Block, J.H. HREELS and TDS studies of NO adsorption and NO + H_2 reaction on Pt (100) surfaces. *Surface science* **1995**, *329* (1-2), 61-70.

(30) Zhang, X.; Wang, X.; Zhao, X.; Xu, Y.; Gao, H.; Zhang, F. An Investigation on N_2O Formation Route over Pt/HY in H_2-SCR. *Chemical Engineering Journal* **2014**, *252*, 288–297.

(31) Conner Jr, W. C.; Falconer, J.L. Spillover in heterogeneous catalysis. *Chemical reviews* **1995**, *95* (3), 759-788.

(32) Shin, H.; Choi, M.; Kim, H. A Mechanistic Model for Hydrogen Activation, Spillover, and Its Chemical Reaction in a Zeolite-Encapsulated Pt Catalyst. *Physical Chemistry Chemical Physics* **2016**, *18* (10), 7035–7041.

(33) Chiarello, G. L.; Ferri, D.; Grunwaldt, J. D.; Forni, L.; Baiker, A. Flame-Synthesized $LaCoO_3$-Supported Pd: 2. Catalytic Behavior in the Reduction of NO by H_2 under Lean Conditions. *J Catal* **2007**, *252* (2), 137–147.

(34) Li, L.; Zhang, F.; Guan, N.; Schreier, E.; Richter, M. NO Selective Reduction by Hydrogen on Potassium Titanate Supported Palladium Catalyst. *Catal Commun* **2008**, *9* (9), 1827–1832.

(35) Komatsubara, M.; Koga, A.; Tanaka, M.; Hagiwara, R.; Iwamoto, M. Three Pathways to Selective Catalytic Reduction of NO over Pt/Nb-AlMCM-41 under H_2 with Excess O_2. *Catal Sci Technol* **2016**, *6* (20), 7398–7407.

(36) Hasegawa, Y.; Haneda, M.; Kintaichi, Y.; Hamada, H. Zn-Promoted Rh/SiO_2 Catalyst for the Selective Reduction of NO with H_2 in the Presence of O_2 and SO_2. *Appl Catal B* **2005**, *60* (1–2), 41–47.

(37) Xue, H.; Li, G.; Liu, P.; Wang, F.; Bai, Y.; Wang, K. Review of Catalysts for Selective Catalytic Reduction (SCR) of NO_x. In *Advanced Materials Research* **2012**, *550*, 119–123.

(38) Shibata, J.; Hashimoto, M.; Shimizu, K. I.; Yoshida, H.; Hattori, T.; Satsuma, A. Factors Controlling Activity and Selectivity for SCR of NO by Hydrogen over Supported Platinum Catalysts. *Journal of Physical Chemistry B* **2004**, *108* (47), 18327–18335.

(39) Olympiou, G. G.; Efstathiou, A. M. Industrial NO_x Control via H_2-SCR on a Novel Supported-Pt Nanocatalyst. *Chemical Engineering Journal* **2011**, *170* (2–3), 424–432.

(40) Shelef, M.; Jones, J.H.; Kummer, J.T.; Otto, K.; Weaver, E.E. Selective catalytic reaction of hydrogen with nitric oxide in the presence of oxygen. *Environmental Science & Technology* **1971**, *5* (9), 790-798.

(41) Fu, L.; Chuang, K. T. Control of Nitrogen Oxide (NO_x) Emissions by Selective Catalytic Reduction with Hydrogen over Hydrophobic Catalysts. *Energy & Fuels* **1989**, *3* (6), 740–743.

(42) Burch, R.; Coleman, M. D. An investigation of the $NO/H_2/O_2$ reaction on noble-metal catalysts at low temperatures under lean-burn conditions. *Applied Catalysis B: Environmental* **1999**, *23* (2-3), 115-121.

(43) Costa, C. N.; Efstathiou, A. M. Mechanistic Aspects of the H_2-SCR of NO on a Novel Pt/MgO-CeO_2 Catalyst. *Journal of Physical Chemistry C* **2007**, *111* (7), 3010–3020.

(44) Yokota, K.; M. Fukui, T_ Tanaka. Catalytic removal of nitric oxide with hydrogen and carbon monoxide in the presence of excess oxygen. *Applied surface science* **1997**, *121*, 273-277.

(45) Zhang, X.; Wang, X.; Zhao, X.; Xu, Y.; Gao, H.; Zhang, F. An Investigation on N_2O Formation Route over Pt/HY in H_2-SCR. *Chemical Engineering Journal* **2014**, *252*, 288–297.

(46) Hong, Z.; Wang, Z.; Chen, D.; Sun, Q.; Li, X. Hollow ZSM-5 Encapsulated Pt Nanoparticles for Selective Catalytic Reduction of NO by Hydrogen. *Appl Surf Sci* **2018**, *440*, 1037–1046.

(47) Yu, Q.; Richter, M.; Kong, F.; Li, L.; Wu, G; Guan, N. Selective catalytic reduction of NO by hydrogen over Pt/ZSM-35. *Catalysis Today* **2010**, *158* (3-4), 452-458.

(48) Li, L.; Wu, P.; Yu, Q.; Wu, G.; Guan, N. Low Temperature H_2-SCR over Platinum Catalysts Supported on Ti-Containing MCM-41. *Appl Catal B* **2010**, *94* (3–4), 254–262.

(49) Yang, S.; Wang, X.; Chu, W.; Song, Z.; Zhao, S. An Investigation of the Surface Intermediates of H2-SCR of NOx over Pt/H-FER. *Appl Catal B* **2011**, *107* (3–4), 380–385.

(50) Satsuma, A.; Hashimoto, M.; Shibata, J.; Yoshida, H.; Hattori, T. Nitrous Oxide Free Pathway for Selective Reduction of NO by Hydrogen over Supported Pt Catalysts. *Chemical Communications* **2003**, *3* (14), 1698–1699.

(51) Yokota, K.; Fukui, M.; Tanaka, T. Catalytic removal of nitric oxide with hydrogen and carbon monoxide in the presence of excess oxygen. *Applied surface science* **1997**, *121*, 273-277.

(52) Nanba, T.; Kohno, C.; Masukawa, S.; Uchisawa, J.; Nakayama, N.; Obuchi, A. Improvements in the N_2 Selectivity of Pt Catalysts in the NO-H_2-O_2 Reaction at Low Temperatures. *Appl Catal B* **2003**, *46* (2), 353–364.

(53) Burch, R.; Millington, P. J.; Walker, A. P. Mechanism of the Selective Reduction of Nitrogen Monoxide on Platinum-Based Catalysts in the Presence of Excess Oxygen. *Appl Catal B* **1994**, *4* (1), 65–94.

(54) Costa, C. N.; Savva, P. G.; Fierro, J. L. G.; Efstathiou, A. M. Industrial H_2-SCR of NO on a Novel Pt/MgO–CeO_2 Catalyst. *Appl Catal B* **2007**, *75* (3–4), 147–156.

(55) Liu, Z.; Lu, Y.; Yuan, L.; Ma, L.; Zheng, L.; Zhang, J.; Hu, T. Selective Catalytic Reduction of NO_x with H_2 over WO_3 Promoted Pt/TiO_2 Catalyst. *Appl Catal B* **2016**, *188*, 189–197.

(56) Engelmann-Pirez, M.; Granger, P.; Leclercq, G. Investigation of the Catalytic Performances of Supported Noble Metal Based Catalysts in the NO + H_2 Reaction under Lean Conditions. In *Catalysis Today* **2005,** *107*, 315–322.

(57) Wen, B., NO reduction with H_2 in the presence of excess O_2 over Pd/MFI catalyst. *Fuel*, **2002**, *81* (14), 1841-1846.

(58) Sterlepper, S.; Fischer, M.; Claßen, J.; Huth, V.; Pischinger, S. Concepts for Hydrogen Internal Combustion Engines and Their Implications on the Exhaust Gas Aftertreatment System. *Energies (Basel)* **2021**, *14* (23).

(59) Ma, D. S.; Sun, Z. Y. Progress on the Studies about NO_x Emission in PFI-H_2ICE. *Int J Hydrogen Energy* **2020**, *45* (17), 10580–10591.

(60) Qing, Y. U.; Fanxiao, K.; Landong, L. I.; Guangjun, W. U.; Naijia, G. Fast Catalytic Reduction of NO_x by H_2 over Pd-Based Catalysts. *J Catal* **2010**, *31* (3), 261–263.

(61) Leicht, M.; Schott, F. J. P.; Bruns, M.; Kureti, S. NO_x Reduction by H_2 on WO_x/ZrO_2-Supported Pd Catalysts under Lean Conditions. *Appl Catal B* **2012**, *117–118*, 275–282.

(62) Schott, F. J. P.; Balle, P.; Adler, J.; Kureti, S. Reduction of NOx by H_2 on $Pt/WO_3/ZrO_2$ Catalysts in Oxygen-Rich Exhaust. *Appl Catal B* **2009**, *87* (1–2), 18–29.

(63) Duan, K.; Chen, B.; Zhu, T.; Liu, Z. Mn Promoted Pd/TiO_2-Al_2O_3 Catalyst for the Selective Catalytic Reduction of NO_x by H_2. *Appl Catal B* **2015**, *176–177*, 618–626.

(64) Savva, P. G.; Efstathiou, A. M. The Influence of Reaction Temperature on the Chemical Structure and Surface Concentration of Active NO_x in H_2-SCR over Pt/MgO{single Bond}CeO_2: SSITKA-DRIFTS and Transient Mass Spectrometry Studies. *J Catal* **2008**, *257* (2), 324–333.

(65) Costa, C. N.; Efstathiou, A. M. Mechanistic Aspects of the H_2-SCR of NO on a Novel Pt/MgO-CeO_2 Catalyst. *Journal of Physical Chemistry C* **2007**, *111* (7), 3010–3020.

(66) Väliheikki, A.; Petallidou, K. C.; Kalamaras, C. M.; Kolli, T.; Huuhtanen, M.; Maunula, T.; Keiski, R. L.; Efstathiou, A. M. Selective Catalytic Reduction of NO by Hydrogen (H_2-SCR) on WO -Promoted Ce Zr_1-O_2 Solids. *Appl Catal B* **2014**, *156–157*, 72–83.

(67) Lykaki, M.; Stefa, S.; Carabineiro, S.; Pandis, P.; Stathopoulos, V.; Konsolakis, M. Facet-Dependent Reactivity of Fe_2O_3/CeO_2 Nanocomposites: Effect of Ceria Morphology on CO Oxidation. *Catalysts* **2019**, *9* (4), 371.

(68) Peng, Z.; Li, Z.; Liu, Y.-Q.; Yan, S.; Tong, J.; Wang, D.; Ye, Y.; Li, S. Supported Pd Nanoclusters with Enhanced Hydrogen Spillover for NO_x Removal via H_2 -SCR: The Elimination of "Volcano-Type" Behaviour. *Chemical Communications* **2017**, *53* (44), 5958–5961.

(69) Savva, Z.; Petallidou, K. C.; Damaskinos, C. M.; Olympiou, G. G.; Stathopoulos, V. N.; Efstathiou, A. M. H_2-SCR of NO_x on Low-SSA CeO_2-Supported Pd: The Effect of Pd Particle Size. *Appl Catal A Gen* **2021**, *615*.

(70) Liu, Z. P.; Jenkins, S. J.; King, D. A. Car Exhaust Catalysis from First Principles: Selective NO Reduction under Excess O_2 Conditions on Ir. *J Am Chem Soc* **2004**, *126* (34), 10746–10756.

(71) Yoshinari, T.; Sato, K.; Haneda, M.; Kintaichi, Y.; Hamada, H. Remarkable promoting effect of coexisting SO_2 on the catalytic activity of Ir/SiO_2 for NO reduction in the presence of oxygen. Catalysis Communications **2001**, *2* (5), 155-158.

(72) Yoshinari, T.; Sato, K.; Haneda, M.; Kintaichi, Y.; Hamada, H. Positive effect of coexisting SO_2 on the activity of supported iridium catalysts for NO reduction in the presence of oxygen. *Applied Catalysis B: Environmental* **2003**, *41* (1-2),157-169.

(73) Liu, Z. P.; Jenkins, S. J.; King, D. A. Step-Enhanced Selectivity of NO Reduction on Platinum-Group Metals. *J Am Chem Soc* **2003**, *125* (48), 14660–14661.

(74) Li, Z.; Navarro, M. T.; Martínez-Triguero, J.; Yu, J.; Corma, A. Synthesis of Nano-SSZ-13 and Its Application in the Reaction of Methanol to Olefins. *Catal Sci Technol* **2016**, *6* (15), 5856–5863.

(75) Ho, P. H.; Yao, D.; Creaser, D.; Olsson, L. Advantages of High-Siliceous Zeolites in the Reactivity and Stability of Diesel Oxidation Catalysts. *ACS Engineering Au* **2022**, *2* (3), 219–235.

(76) Wijayanti, K.; Andonova, S.; Kumar, A.; Li, J.; Kamasamudram, K.; Currier, N. W.; Yezerets, A.; Olsson, L. Impact of Sulfur Oxide on NH_3-SCR over Cu-SAPO-34. *Appl Catal B* **2015**, *166–167*, 568–579.

(77) Ho, P. H.; Shao, J.; Yao, D.; Ilmasani, R. F.; Salam, M. A.; Creaser, D.; Olsson, L. The Effect of Pt/Pd Ratio on the Oxidation Activity and Resistance to Sulfur Poisoning for Pt-Pd/BEA Diesel Oxidation Catalysts with High Siliceous Content. *J Environ Chem Eng* **2022**, *10* (4).

(78) Yao, D.; Feizie Ilmasani, R.; Wurzenberger, J. C.; Glatz, T.; Han, J.; Wang, A.; Creaser, D.; Olsson, L. Kinetic Modeling of CO Assisted Passive NO_x Adsorption on Pd/SSZ-13. *Chemical Engineering Journal* **2022**, *428*.

(79) Rappé, K. G.; DiMaggio, C.; Pihl, J. A.; Theis, J. R.; Oh, S. H.; Fisher, G. B.; Parks, J.; Easterling, V. G.; Yang, M.; Stewart, M. L.; Howden, K. C. Aftertreatment Protocols for Catalyst Characterization and Performance Evaluation: Low-Temperature Oxidation, Storage, Three-Way, and NH_3-SCR Catalyst Test Protocols. *Emission Control Science and Technology* **2019**, *5* (2), 183–214.

(80) Brunauer, S.; Emmett, P.H.; Teller, E. Adsorption of gases in multimolecular layers. *Journal of the American chemical society* **1938**, *60* (2), 309-319.

(81) Pope, C.G. X-ray diffraction and the Bragg equation. *Journal of chemical education* **1997**, *74* (1), 129.

(82) Freel, J. Chemisorption on supported platinum: II. Stoichiometry for hydrogen, oxygen and carbon monoxide. *Journal of Catalysis* **1972**, *25* (1), 149-160.

(83) Allian, A. D.; Takanabe, K.; Fujdala, K. L.; Hao, X.; Truex, T. J.; Cai, J.; Buda, C.; Neurock, M.; Iglesia, E. Chemisorption of CO and Mechanism of CO Oxidation on Supported Platinum Nanoclusters. *J Am Chem Soc* **2011**, *133* (12), 4498–4517.

(84) Canton, P.; Fagherazzi, G.; Battagliarin, M.; Menegazzo, F.; Pinna, F.; Pernicone, N. Pd/CO Average Chemisorption Stoichiometry in Highly Dispersed Supported Pd/γ-Al_2O_3 Catalysts. *Langmuir* **2002**, *18* (17), 6530–6535.

(85) Krishnamurthy, S.; Landolt, G.R.; Schoennagel, H.J. The stoichiometry of hydrogen and CO chemisorption on Ir γ-Al_2O_3. Journal of Catalysis **1982**, *78* (2), 319-326.

(86) Ivanova, E.; Mihaylov, M.; Thibault-Starzyk, F.; Daturi, M.; Hadjiivanov, K. FTIR Spectroscopy Study of CO and NO Adsorption and co-Adsorption on Pt/TiO_2. *J Mol Catal A Chem* **2007**, *274* (1–2), 179–184.

(87) Dulaurent, O.; Bianchi, D. Adsorption isobars for CO on a Pt/Al_2O_3 catalyst at high temperatures using FTIR spectroscopy: isosteric heat of adsorption and adsorption model. *Applied Catalysis A: General* **2000**, *196* (2), 71-280.

(88) Sing, K.S. Reporting physisorption data for gas/solid systems with special reference to the determination of surface area and porosity (Recommendations 1984). *Pure and applied chemistry* **1985**, *57* (4), 603-619.

(89) Bera, P.; Priolkar, K. R.; Gayen, A.; Sarode, P. R.; Hegde, M. S.; Emura, S.; Kumashiro, R.; Jayaram, V.; Subbanna, G. N. Ionic Dispersion of Pt over CeO_2 by the Combustion Method: Structural Investigation by XRD, TEM, XPS, and EXAFS. *Chemistry of Materials* **2003**, *15* (10), 2049–2060.

(90) Liu, H. H.; Wang, Y.; Jia, A. P.; Wang, S. Y.; Luo, M. F.; Lu, J. Q. Oxygen Vacancy Promoted CO Oxidation over Pt/CeO_2 Catalysts: A Reaction at Pt-CeO_2 Interface. *Appl Surf Sci* **2014**, *314*, 725–734.

(91) Chastain, J.; King Jr, R.C. *Handbook of X-ray photoelectron spectroscopy.* Perkin-Elmer Corporation **1992**, 40, pp.221.